SECURITY INFORMATION

[redacted]

Copy 210
RM L52E15

[redacted]

TECH LIBRARY KAFB, NM
0144366

NACA RM L52E15

7337

NACA

RESEARCH MEMORANDUM

WIND-TUNNEL INVESTIGATION OF A RAM-JET CANARD MISSILE MODEL HAVING A WING AND CANARD SURFACES OF DELTA PLAN FORM WITH 70° SWEPT LEADING EDGES

LONGITUDINAL AND LATERAL STABILITY AND CONTROL CHARACTERISTICS AT A MACH NUMBER OF 1.60

By M. Leroy Spearman and Ross B. Robinson

Langley Aeronautical Laboratory
Langley Field, Va.

[redacted]

NATIONAL ADVISORY COMMITTEE FOR AERONAUTICS

WASHINGTON

August 1, 1952

319.98/13

[redacted]

Classification cancelled (or changed to UNCLASSIFIED)

By authority of NASA ~~[illegible]~~ TECH PUB ANNOUNCEMENT #115
(OFFICER AUTHORIZED TO CHANGE)

By ..... 22 May 57
NAME AND

NMP
GRADE OF OFFICER MAKING CHANGE)

3 Apr 61
DATE

TECH LIBRARY KAFB, NM
0144366

NATIONAL ADVISORY COMMITTEE FOR AERONAUTICS

RESEARCH MEMORANDUM

WIND-TUNNEL INVESTIGATION OF A RAM-JET CANARD MISSILE MODEL HAVING A WING AND CANARD SURFACES OF DELTA PLAN FORM WITH 70° SWEPT LEADING EDGES

LONGITUDINAL AND LATERAL STABILITY AND CONTROL CHARACTERISTICS AT A MACH NUMBER OF 1.60

By M. Leroy Spearman and Ross B. Robinson

SUMMARY

An investigation has been conducted in the Langley 4- by 4-foot supersonic pressure tunnel to determine the longitudinal and lateral stability and control characteristics of a ram-jet canard missile having a center-of-gravity location of -19.5 percent of the wing mean aerodynamic chord. The tests were made at a Mach number of 1.60 and a Reynolds number of 3.83×10^6 based on the wing mean aerodynamic chord. The model had a wing and vertical and horizontal canard surfaces of delta plan form with 70° swept leading edges. Nacelles were mounted in the vertical plane on unswept pylons near the rear of the model. The effects of vertical-canard size and nacelle longitudinal location on the stability characteristics were also investigated.

All configurations were found to be longitudinally stable with a static margin of about .14 percent of the wing mean aerodynamic chord. A maximum trim angle of attack of 11.5° and trim lift coefficient of 0.42 was obtainable with the maximum horizontal-canard deflection of 12°.

With the large vertical canard and the forward nacelle location, the model was directionally unstable. Reducing the canard size or moving the nacelle and strut rearward resulted in a directionally stable model. For the configuration with the small vertical canard and the forward nacelle location, a maximum sideslip angle of about 9.3° was obtained at zero angle of attack for a vertical-canard deflection of -12°.

The model had a negative dihedral effect that became more negative with increasing angle of attack. The rolling-moment coefficient due to aileron deflection was insufficient to stabilize the model in roll beyond a sideslip angle of 5° at an angle of attack of 6.3°.

INTRODUCTION

Tests have been made in the Langley 4- by 4-foot supersonic pressure tunnel to determine the aerodynamic characteristics of a ram-jet canard missile model at a Mach number of 1.60. These tests were part of a coordinated research program with the Langley Pilotless Aircraft Research Division.

The model had a wing and canard surfaces of delta plan form with 70° swept leading edges. Nacelles were mounted in the vertical plane on short unswept pylons near the rear of the body. The model was equipped with all-movable canard surfaces for both pitch and yaw control and movable wing-tip ailerons for roll control. Six-component force and moment measurements were made as well as hinge-moment measurements for the canard and aileron controls through an angle-of-attack and angle-of-sideslip range. The model center of gravity was located at -19.5 percent of the mean aerodynamic chord. Various component parts of the model could be removed or changed in order to facilitate the investigation of general interference effects between different components and to permit the investigation of various modifications to the basic configuration.

Different phases of the investigation have been concerned with the stability and control characteristics of the complete model, the aerodynamic characteristics of various combinations of components of the model, the effects of nose shape, the effects of canard size, and the effects of nacelle location. This paper presents results of tests of the complete model made at a Mach number of 1.60 and a Reynolds number of 3.83×10^{6} (based on the wing mean aerodynamic chord) to determine the stability and control characteristics of various configurations in both pitch and sideslip. The tests correspond to a power-off condition with air flow through the nacelles.

COEFFICIENTS AND SYMBOLS

The results of the tests are presented as standard NACA coefficients of forces and moments. The data are referred to the stability-axes system (fig. 1) with the reference center of gravity at -19.5 percent of the wing mean aerodynamic chord.

The coefficients and symbols are defined as follows:

C_L	lift coefficient $(-Z/qS)$
C_X	longitudinal-force coefficient (X/qS)
C_Y	lateral-force coefficient (Y/qS)
C_l	rolling-moment coefficient (L/qSb)
C_m	pitching-moment coefficient $(M'/qS\bar{c})$
C_n	yawing-moment coefficient (N/qSb)
C_{h_H}	horizontal-canard hinge-moment coefficient $\left(H_H/qS_H\bar{c}_H\right)$
C_{h_a}	aileron hinge-moment coefficient $\left(H_a/qS_a\bar{c}_a\right)$
X	force along X-axis
Y	force along Y-axis
Z	force along Z-axis
L	moment about X-axis
M'	moment about Y-axis
N	moment about Z-axis
H_H	moment about horizontal-canard hinge axis
H_a	moment about aileron hinge axis
q	free-stream dynamic pressure
S	total wing area including body intercept
S_H	exposed area of horizontal canard
S_a	aileron area
b	wing span
$\bar{c}$	wing mean aerodynamic chord

$\bar{c}_H$	horizontal-canard mean aerodynamic chord
$\bar{c}_a$	aileron mean aerodynamic chord
M	Mach number
L/D	lift-drag ratio $\left(C_L/-C_X\right)$
ΔC_X	rise in longitudinal-force coefficient above minimum
n_p	neutral-point location, percent $\bar{c}$
α	angle of attack, deg
β	angle of sideslip, deg
δ_H	horizontal-canard deflection, deg
δ_v	vertical-canard deflection, deg
δ_a	aileron deflection, deg
$C_{Y_\beta} = \frac{\partial C_Y}{\partial \beta}$	
$C_{n_\beta} = \frac{\partial C_n}{\partial \beta}$	
$C_{l_\beta} = \frac{\partial C_l}{\partial \beta}$	
$C_{m_{\delta_H}} = \frac{\partial C_m}{\partial \delta_H}$	
$C_{h_{\delta_H}} = \frac{\partial C_{n_H}}{\partial \delta_H}$	
$\left(\alpha_{\delta_H}\right)_{trim}$	rate of change of trim angle of attack with horizontal-canard deflection, $\partial\alpha/\partial\delta_H$

$\left(C_{L_{\delta_H}}\right)_{trim}$ rate of change of lift coefficient with horizontal-canard deflection, $\partial C_L/\partial \delta_H$, measured for $C_m = 0$

$C_{n_{\delta_v}} = \dfrac{\partial C_n}{\partial \delta_v}$

$\beta_{\delta_v} = \dfrac{\partial \beta}{\partial \delta_v}$

$C_{l_{\delta_a}} = \dfrac{\partial C_l}{\partial \delta_a}$

MODEL AND APPARATUS

A three-view drawing of the model is shown in figure 2 and a photograph of the model is shown as figure 3. The geometric characteristics of the model are presented in table I.

The model was composed of a parabolic nose followed by a frustrum of a cone which was faired into a cylinder. Coordinates for the body are given in table II. Canard surfaces in both the vertical and horizontal planes had delta plan forms with 70° swept leading edges. Two different vertical canards were used. Details of the canards are shown in figure 4. The canards were all-movable and were deflected about an axis normal to the body center line. The main wing, located in the horizontal plane, also was of delta plan form with a 70° swept leading edge and had hexagonal sections. Tip ailerons of triangular plan form were separated from the main wing by a small gap parallel to the body center line. A discontinuity in airfoil thickness existed at the parting line between the aileron and the main wing (see fig. 4). The ailerons were deflected about an axis normal to the body center line. Deflections of the ailerons and the vertical canard were made manually with the surfaces being held in position by means of clamping screws. The horizontal canard was motor-driven and deflections could be set remotely.

Force measurements were made through the use of a six-component internal strain-gage balance. Individual strain-gage balances were used to measure the aileron and the horizontal-canard hinge moments.

The model was mounted in the tunnel on a 6° bent sting. Details of the installation are shown in figure 5. Through the use of the bent

sting, it was possible to test through the angle-of-attack range at sideslip angles of 0° and 6° and through the angle-of-sideslip range at angles of attack of 0° and 6°.

The tests were conducted in the Langley 4- by 4-foot supersonic pressure tunnel described in reference 1.

TESTS

Test Conditions

The conditions for the tests were:

Mach number	1.60
Reynolds number, based on wing M.A.C.	3.83×10^{6}
Stagnation dew point, $^{\circ}F$	<-25
Stagnation pressure, atm	1.0
Stagnation temperature, $^{\circ}F$	110

CORRECTIONS AND ACCURACY

The angles of attack and sideslip were corrected for the deflection of the balance under load. The Mach number variation in the test section was ±0.01 and the flow-angle variation in the vertical and horizontal planes was $\pm 0.1^{\circ}$. No corrections were applied to the data to account for these flow variations.

The estimated errors in the individual measured quantities are as follows:

C_L	±0.004
C_X	±0.0023
C_m	±0.0004
C_Y	±0.001
C_n	±0.0005
C_l	±0.0004
C_{h_H}	±0.0005
C_{h_a}	±0.0002
α, deg	±0.1
β, deg	±0.1
δ_H, deg	±0.1
δ_V, deg	±0.1
δ_a, deg	±0.1

The base pressure was measured and the longitudinal-force data were corrected to a base pressure equal to the free-stream static pressure. Errors in the base-pressure measurements are included in the estimated error of C_X.

RESULTS AND DISCUSSION

Presentation of Data

Results are presented for four variations of the test model that differed in the size of the vertical canard surface and in the nacelle location. Two vertical-canard sizes were used, one having half the area of the other, and two longitudinal locations of the nacelle and pylon were used.

A table of the figures presenting the results is given below.

Figure

Longitudinal characteristics:
- Variation of angle of attack, pitching-moment coefficient, longitudinal-force coefficient, and horizontal-canard hinge-moment coefficient with lift coefficient and horizontal-canard deflection for various configurations 6
- Variation of pitching-moment coefficient and horizontal-canard hinge-moment coefficient with angle of attack and horizontal-canard deflection for various configurations 7
- Longitudinal characteristics for trim ($C_m = 0$) 8
- Trim lift-drag ratios ($C_m = 0$) 9
- Drag variation due to lift, ΔC_X against C_L^2 10
- Variation of neutral-point location with lift coefficient 11
- Variation of pitching-moment coefficient and horizontal-canard hinge-moment coefficient with horizontal-canard deflection and angle of attack for various configurations 12
- Variation of trim longitudinal characteristics with horizontal-canard deflection 13
- Variation of normal acceleration with horizontal-canard deflection 14

Figure

Lateral characteristics:
Variation of yawing-moment coefficient, lateral-force coefficient, and rolling-moment coefficient with angle of sideslip for various configurations 15
Effect of angle of attack on the sideslip characteristics for model with small vertical canard and forward nacelle location . . . . . 16 to 18
Directional control characteristics for model with large vertical canard and forward nacelle location 19
Directional control characteristics for model with small vertical canard and forward nacelle location . . . . . 20 and 21
Aileron characteristics for model with large vertical canard and forward nacelle location . . . . . 22 to 24

Longitudinal Characteristics

Lift and longitudinal force.- The trim-lift curve (fig. 8) is nearly linear with an average lift-curve slope C_{L_α} of about 0.032 in the positive C_L range. This value is in good agreement with the linear-theory value of C_{L_α} of 0.034 for the wing alone as obtained by the method of reference 2. There is only a slight effect of vertical-canard size or nacelle location on the lift-curve slope but higher maximum trim lift coefficients were obtained for the model with the forward nacelle location.

The fact that the longitudinal-force coefficient for the model with the small vertical canard is higher than that for the model with the large vertical canard is probably a result of the higher thickness ratio and the altered section of the smaller canard and would not be expected to occur if the thickness ratios and sections were the same for the two canards.

The longitudinal-force due-to-lift parameter $\Delta C_X/C_L^2$ is constant and is approximately the same for all configurations (fig. 10). The value of $\Delta C_X/C_L^2$ is about 0.54, which is in agreement with the value indicated by the average experimental $\frac{1}{57.3C_{L_\alpha}}$.

A maximum trim lift-drag ratio of about 3 at a C_L of 0.34 was obtained for the model with the large vertical canard (fig. 9). A slightly lower value of L/D was obtained for the configurations having

the small vertical canard but this would not be expected if the large and small canards had the same thickness ratios and sections.

Static longitudinal stability.- The missile is longitudinally stable throughout the trim-lift range for each configuration with a static margin of about 14 percent mean aerodynamic chord near zero lift (fig. 11). There is little effect of vertical-canard size on the longitudinal stability but the model with the rearward nacelle location shows a greater increase in stability with increasing C_L than does the model with the forward nacelle location.

The importance of trimmed longitudinal data is shown by the fact that the pitching-moment curves for $\delta_H = 0$ (for example see fig. 6(a)) indicate the possibility of approximately neutral stability near maximum lift, whereas the trim pitching-moment curve $\left(\delta_H = 12^\circ\right)$ indicates greater stability near maximum trim lift than at zero lift. There is some indication from the shape of the pitching-moment curves that, if higher trim lifts were attainable through the use of greater canard deflections or through a change in the center-of-gravity location, then the model may become neutrally stable or unstable.

Longitudinal control characteristics.- The variation of pitching-moment coefficient and horizontal-canard hinge-moment coefficient with horizontal-canard deflection for various angles of attack (fig. 12) indicate a decrease in $C_{m_{\delta_H}}$ and $C_{h_{\delta_H}}$ with increasing angle of attack. There is no appreciable effect of vertical-canard size or nacelle location on $C_{m_{\delta_H}}$ or $C_{h_{\delta_H}}$.

The theoretical curve shown in figure 12 was obtained by the method of reference 2 for an isolated delta wing. The lower experimental value of $C_{h_{\delta_H}}$ is probably due to the gap between the deflected canard and the body and differences in the effects of the body flow field on the canard surfaces. The theoretical variations of C_{h_H} with C_L (fig. 6(a)) and C_{h_H} with α (fig. 7(a)) for the canard and body moving as a unit agree closely with the experimental results.

The horizontal-canard effectiveness parameters $\left(\alpha_{\delta_H}\right)_{trim}$ and $\left(C_{L_{\delta_H}}\right)_{trim}$ (fig. 13) are linear only for small deflections (about 3°) where the value of $\left(\alpha_{\delta_H}\right)_{trim}$ is about 1.7 and the value of $\left(C_{L_{\delta_H}}\right)_{trim}$ is about 0.052. The nonlinear variations of α_{trim} and $C_{L_{trim}}$ for

higher deflections occur as a result of the changes in static longitudinal stability; that is, there is a reduction in the control effectiveness (ability of the control to change the trim attitude) in the region of increased stability and an increase in control effectiveness in the region of decreased stability. With the maximum horizontal-canard deflection of 12°, the maximum trim angle of attack is 11.5° and the corresponding trim C_L is about 0.42 for the model with the forward nacelle location; whereas, for the model with the rearward nacelle location, the maximum trim α is about 10° with a trim C_L of about 0.38. The indications are that higher trim angles and trim lifts may be obtained with higher horizontal-canard deflections but, as already pointed out, the missile may become longitudinally unstable before any appreciable increase in α or C_L could be obtained.

The trim-lift data from figure 13 were used to obtain the variation of normal acceleration with horizontal-canard deflection for various lift coefficients as shown in figure 14. For low trim lift coefficients, of course, large accelerations are possible, but the maneuverability decreases rapidly as the lift coefficient is increased because of the low maximum trim lift coefficients obtainable. The maneuverability of the three configurations varies according to their static stability - the model having the rearward nacelle location being the least maneuverable and the most stable.

Lateral Characteristics

Sideslip derivatives.- Although there is little effect of vertical-canard size or nacelle location on the variation of lateral-force coefficient or rolling-moment coefficient with sideslip angle at zero angle of attack, there is a large effect on the yawing-moment coefficient. (See fig. 15.) The model with the large vertical canard and the forward nacelle location is directionally unstable. Although this model could be made directionally stable by moving the center of gravity forward, this would not be desirable because of the nonlinear nature of the yawing-moment curve and because of the attendant increase in longitudinal stability. Since this nonlinear yawing-moment curve probably results from the effects of canard sidewash on the nacelle installations it would seem more reasonable to change the directional characteristics by moving the nacelles rearward or by reducing the size of the vertical canards. With the rearward nacelle location or with the small vertical canard, the model becomes directionally stable (see fig. 15) and the most stable configuration is that having both the rearward nacelle location and the small vertical canard. The yawing-moment curves for the models with the forward nacelle location have nonlinear variations with sideslip angle that essentially disappear for the models with the rearward nacelle location.

The effect of angle of attack on the sideslip characteristics of the model with the small vertical canard and forward nacelle (fig. 16) indicates a slight decrease in C_{Y_β}, a slight increase in C_{n_β} and a positive increase in C_{l_β} (negative dihedral effect) as the angle of attack is changed from 0° to 6.3°. The difference shown by the two runs at $\alpha = 6.3^\circ$ probably results from differences in the angular setting of the canards. The variation of C_Y, C_n, and C_l with C_L for sideslip angles of 0° and 6.3° (fig. 17) was used to determine the slopes of C_{Y_β}, C_{n_β}, and C_{l_β} between these two angles (fig. 18). These slopes are not in exact agreement with slopes measured for small sideslip angles from figure 16 since C_Y, C_n, and C_l do not vary linearly with β; however, the slopes shown in figure 18 are sufficient to indicate the probable variation of the sideslip derivatives throughout the lift range. These variations show a continual decrease in C_{Y_β} with increasing C_L, an initial increase in the directional stability C_{n_β} with an indication of decreasing C_{n_β} for higher lifts, and a continual increase in C_{l_β} (negative dihedral effect) throughout the C_L range shown.

Directional control.- The directional control characteristics were investigated only for the model with the forward nacelle and with both the large and small vertical canards. The directionally unstable model (large vertical canards) is, of course, quite sensitive in yaw to vertical-canard deflections. The variation of yawing-moment coefficient with vertical-canard deflection obtained from figure 19(a) for various sideslip angles is shown in figure 19(c).

The effects of vertical-canard deflection on the lateral characteristics of the model with the small vertical canard and forward nacelle at $\alpha = 0^\circ$ and 6.3° (fig. 20) show considerable nonlinearity in the yawing-moment curves. The directional control characteristics summarized in figure 21 indicate an average value of $C_{n_{\delta_v}}$ at $\beta = 0^\circ$ of about 0.003 for both angles of attack. The variation of C_n with C_L for δ_v of 0° and -4° at $\beta \approx 6^\circ$ (fig. 17) indicates an essentially constant value of $C_{n_{\delta_v}}$. The variation of trim β with δ_v (fig. 21(b)) is somewhat nonlinear with an average value of β_{δ_v} at small deflections of about 0.78. A maximum sideslip angle of about 9.3° is obtainable at $\alpha = 0^\circ$ and about 8.5° at $\alpha = 6.3^\circ$ with the maximum vertical-canard deflection of -12°.

No hinge-moment measurements were made for the vertical canards, but it is reasonable to assume that at least for the large vertical canard they would be similar to those for the horizontal canard inasmuch as the plan form and hinge-line location for the horizontal and vertical canards are the same.

Aileron characteristics.- The aileron characteristics (fig. 22) are for the model with the forward nacelle location and the large vertical canard. For most of these tests, the left aileron was deflected through a range of $\pm 10^{\circ}$ while the right aileron was kept at zero deflection. Aileron characteristics were not determined for any of the other configurations. The size of the vertical canard would probably have a negligible effect on the aileron characteristics inasmuch as breakdown tests of the model have shown no effect of the canards on the wing. The effect of nacelle location on the aileron characteristics is not known; however, for the Mach number of these tests the shock from the nacelle lies completely ahead of the aileron for both the forward and the rearward nacelle locations.

The rolling moment produced by the aileron is nearly linear through the angle-of-attack range with a decrease in $C_{l_{\delta_a}}$ occurring as the angle of attack increases. The adverse yawing moment increases with increasing angle of attack and there is little change in the aileron hinge-moment coefficient with angle of attack. The variation of C_n and C_h with α is similar to that shown in reference 3 for a similar wing and aileron at $M = 1.90$.

In order to investigate the possibility of combined interference effects resulting from the deflection of left and right ailerons simultaneously, one test was made with the left aileron deflected 4° and the right aileron deflected -4°. These results are shown in figure 23 together with the results for the $\pm 4^{\circ}$ deflections of the left aileron only. The dashed line shown in this figure was obtained by adding the results of the $\pm 4^{\circ}$ deflections of the left aileron. A comparison of the results shown by the dashed line with the results of the test wherein both left and right ailerons were deflected shows practically no change in the rolling-moment coefficients. However, more adverse yaw was obtained when both ailerons are deflected than was obtained by the addition of the C_n values for the positive and negative deflections of the same aileron, possibly as a result of differences in interference effects of the aileron flow field on the nacelle installations.

There is little variation in aileron hinge-moment coefficient with aileron deflection (fig. 24) and the trends shown are quite similar to those shown in references 3 and 4 for similar wings and controls at $M = 1.90$ and those shown in reference 5 for a 60° delta wing with a

half-delta tip aileron at supersonic speeds. The variation of rolling-moment coefficient with aileron deflection (fig. 24) is fairly linear and is in good agreement with that predicted by the method of reference 6. The rolling power of the ailerons does not appear to be sufficient to stabilize the missile in roll completely. For example, at $\alpha = 6.3^{\circ}$ the maximum sideslip angle obtainable with maximum vertical-canard deflection is 8.5° (fig. 21) and the induced rolling-moment coefficient for this condition is about 0.012. The maximum rolling-moment coefficient produced by the ailerons $\left(\delta_a = \pm 10^{\circ}\right)$ for this angle of attack is only about 0.0075. The maximum sideslip angle for which the aileron is powerful enough to trim is about 5°.

There is some nonlinearity in the variation of C_L with δ_a (fig. 24), but within the accuracy of the data the average value of $C_{L_{\delta_a}}$ is essentially in agreement with the theoretical value obtained by the method of reference 6. The pitching-moment coefficient variation with δ_a is quite linear and is somewhat greater than that predicted by the method of reference 6.

CONCLUSIONS

An investigation has been made to determine the longitudinal and lateral stability and control characteristics of a ram-jet canard missile having a center-of-gravity location of -19.5 percent of the wing mean aerodynamic chord. The tests were made at a Mach number of 1.60 and a Reynolds number of 3.83×10^6 based on the wing mean aerodynamic chord. An analysis of the results indicated the following conclusions:

1. All configurations were longitudinally stable with a static margin of about 14 percent of the wing mean aerodynamic chord.

2. With the maximum horizontal-canard deflection of 12°, a trim angle of attack of 11.5° and a trim lift coefficient of about 0.42 were obtained for the models having the forward nacelle location and a trim angle of attack of 10° and a trim lift coefficient of about 0.38 were obtained for the model with the rearward nacelle location.

3. A maximum trim lift-drag ratio of about 3 was obtained at a lift coefficient of 0.34.

4. With the large vertical canard and the forward nacelle location, the model was directionally unstable. Reducing the canard size or moving the nacelle rearward resulted in a directionally stable configuration.

5. For the model with the small vertical canard and the forward nacelle location, a maximum sideslip angle of about 9.3° was obtained at zero angle of attack for a vertical-canard deflection of -12°.

6. The model with the small vertical canard and the forward nacelle location had a negative dihedral effect that became more negative with increasing angle of attack or lift coefficient.

7. The rolling-moment coefficient due to aileron deflection was in good agreement with the theoretically determined value but was insufficient to stabilize the model in roll beyond a sideslip angle of 5° at an angle of attack of 6.3°.

Langley Aeronautical Laboratory
National Advisory Committee for Aeronautics
Langley Field, Va.

REFERENCES

1. Robinson, Ross B., and Driver, Cornelius: Aerodynamic Characteristics at Supersonic Speeds of a Series of Wing-Body Combinations Having Cambered Wings With an Aspect Ratio of 3.5 and a Taper Ratio of 0.2. Effects of Sweep Angle and Thickness Ratio on the Aerodynamic Characteristics in Pitch at $M = 1.60$. NACA RM L51K16a, 1952.

2. Ribner, Herbert S., and Malvestuto, Frank S., Jr.: Stability Derivatives of Triangular Wings at Supersonic Speeds. NACA Rep. 908, 1948. (Supersedes NACA TN 1572.)

3. Conner, D. William, and May, Ellery B., Jr.: Control Effectiveness Load and Hinge-Moment Characteristics of a Tip Control Surface on a Delta Wing at a Mach Number of 1.9. NACA RM L9H05, 1949.

4. Conner, D. William, and May, Ellery B., Jr.: Control Effectiveness and Hinge-Moment Characteristics of a Tip Control Surface on a Low-Aspect-Ratio Pointed Wing at a Mach Number of 1.9. NACA RM L9H26, 1949.

5. Martz, C. William, and Church, James D.: Flight Investigation at Subsonic, Transonic, and Supersonic Velocities of the Hinge-Moment Characteristics, Lateral-Control Effectiveness, and Wing Damping in Roll of a 60° Sweptback Delta Wing With Half-Delta Tip Ailerons. NACA RM L51G18, 1951.

6. Kainer, Julian H., and King, Mary Dowd: The Theoretical Characteristics of Triangular-Tip Control Surfaces at Supersonic Speeds. Mach Lines Behind Trailing Edges. NACA TN 2715, 1952.

TABLE I

GEOMETRIC CHARACTERISTICS OF MODEL

Body:	
Maximum diameter, in.	2.666
Length, in.	50.833
Fineness ratio	19.067
Base area, sq in.	5.583
Wing:	
Span, in.	11.853
Chord at body center line, in.	17.069
Chord at body intersection, in.	13.407
Chord at aileron break line, in.	4.606
Area (including that within body) sq in.	100.049
Area (exposed), sq in.	59.424
Aspect ratio	1.404
Sweep angle of leading edge, deg	70
Thickness ratio at body center line	.0147
Thickness ratio at aileron break line	.0543
Leading-edge angle normal to leading edge, deg	15.6
Mean aerodynamic chord, in.	11.48
Aileron:	
Area, sq in.	3.201
Mean aerodynamic chord, in.	3.071
Thickness ratio at break line	.039
Large canards:	
Area (exposed), sq in.	6.406
Aspect ratio	1.73
Sweep angle of leading edge, deg	70
Mean aerodynamic chord, in.	2.576
Small canards:	
Area (exposed), sq in.	3.203
Aspect ratio	1.73
Sweep angle of leading edge, deg	70
Mean aerodynamic chord, in.	1.821

TABLE II

BODY COORDINATES

Body station	Radius
0	0
.297	.076
.627	.156
.956	.233
1.285	.307
1.615	.378
1.945	.445
2.275	.509
2.605	.573
2.936	.627
3.267	.682
3.598	.732
3.929	.780
4.260	.824
4.592	.865
4.923	.903
5.255	.940
5.587	.968
5.920	.996
6.252	1.020
6.583	1.042 } conical section
11.542	1.333 }
50.833	1.333 } cylindrical

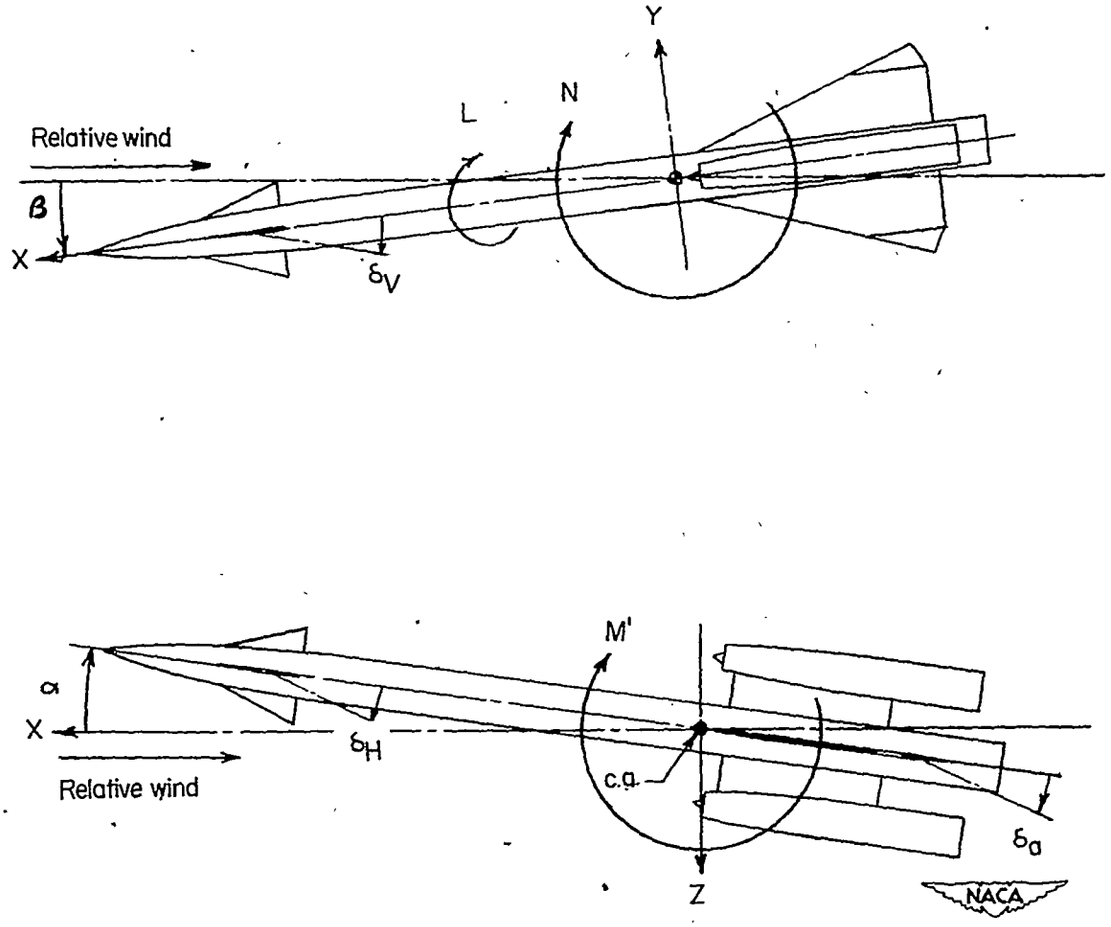

Figure 1.- System of stability axes. Arrows indicate positive values.

[redacted]

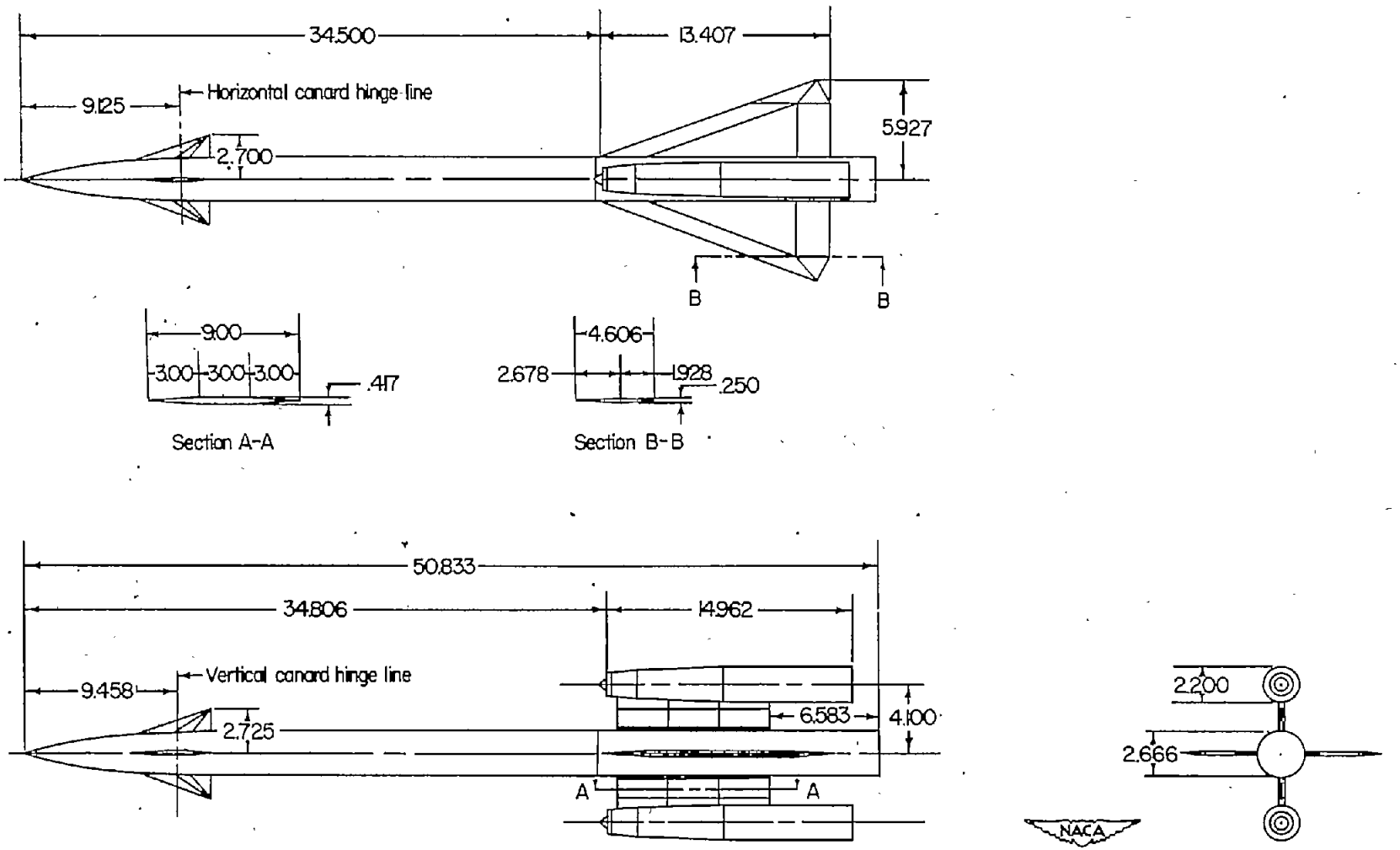

Figure 2.- Details of ram-jet canard missile model. All dimensions are in inches.

[redacted]

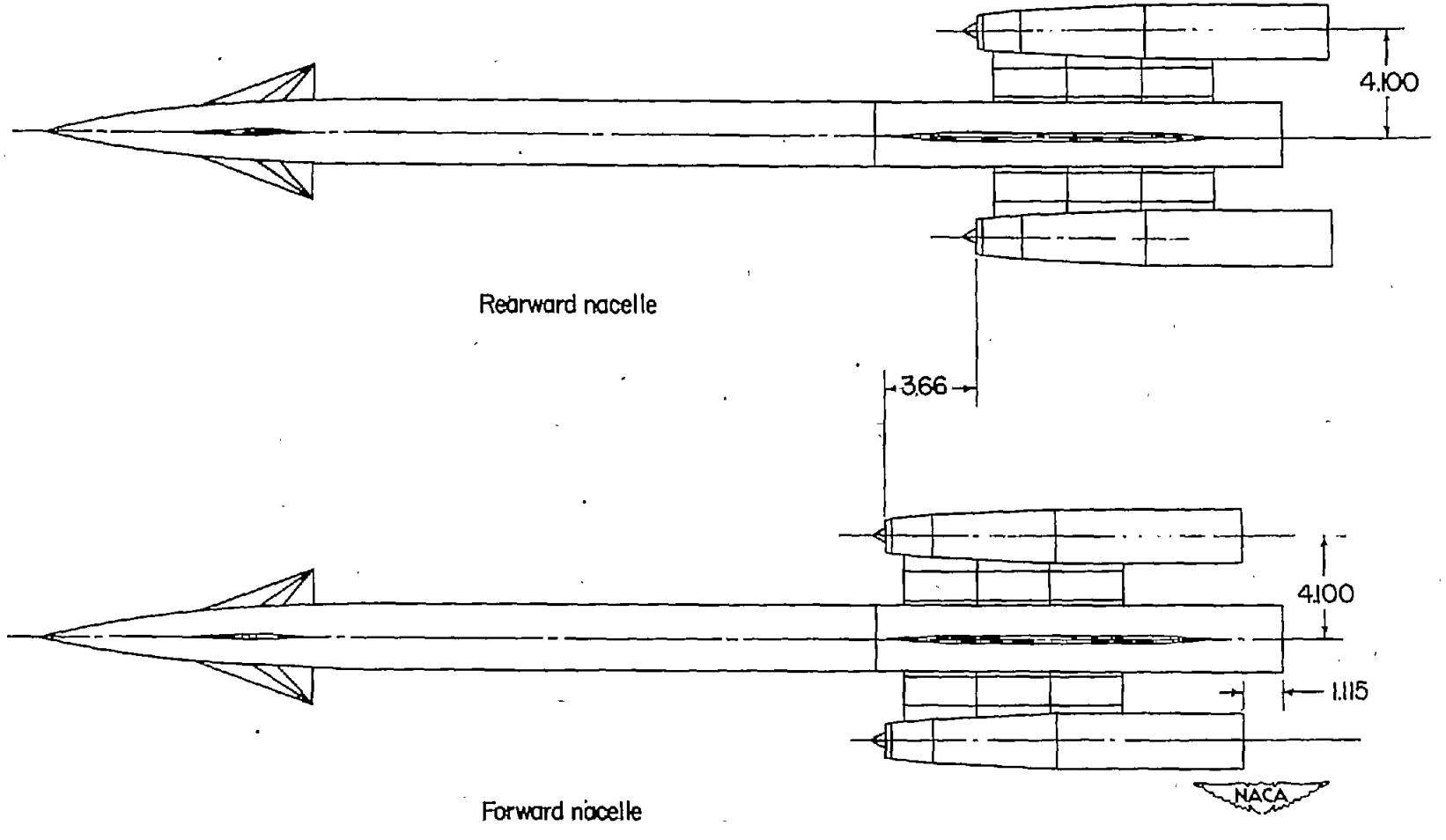

Figure 2.- Concluded.

[redacted]

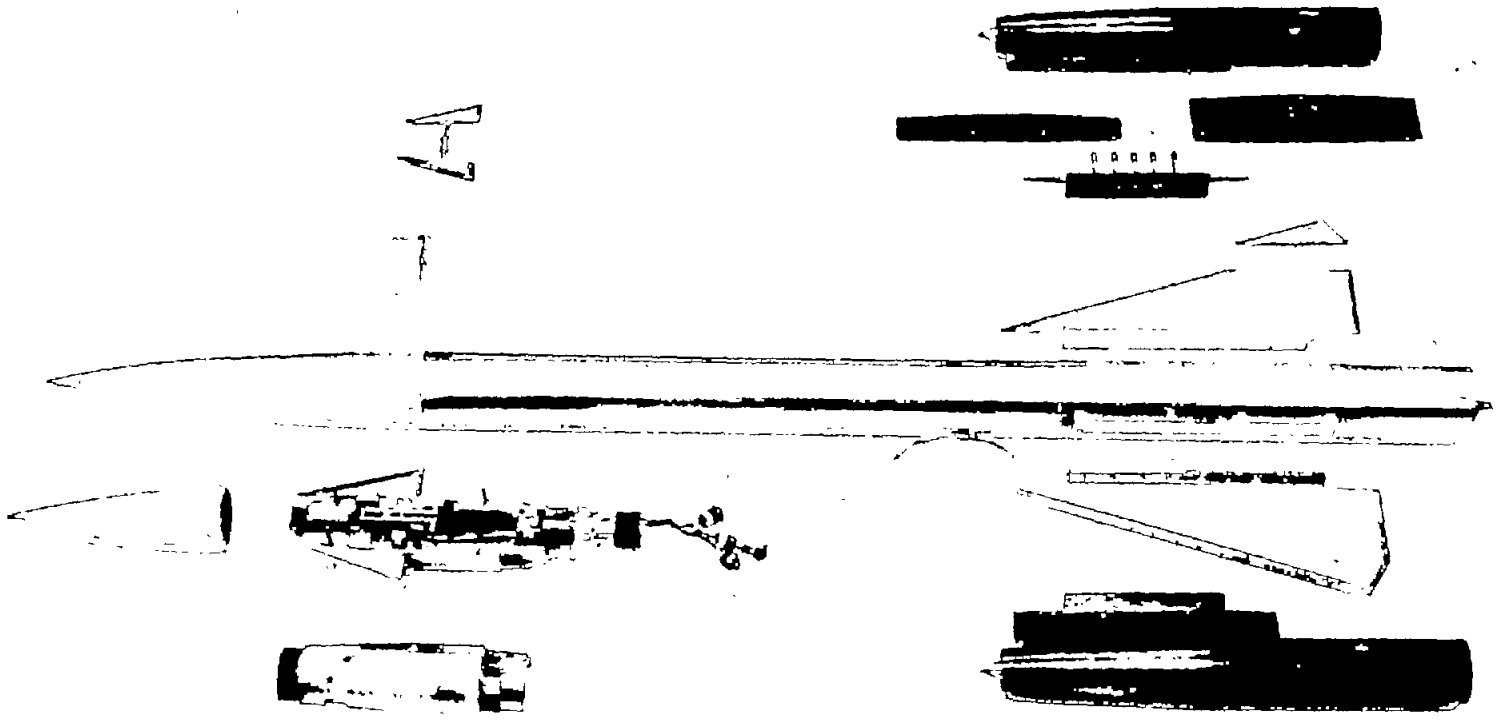

[redacted]

L-74957

Figure 3.- Component parts of ram-jet canard missile model.

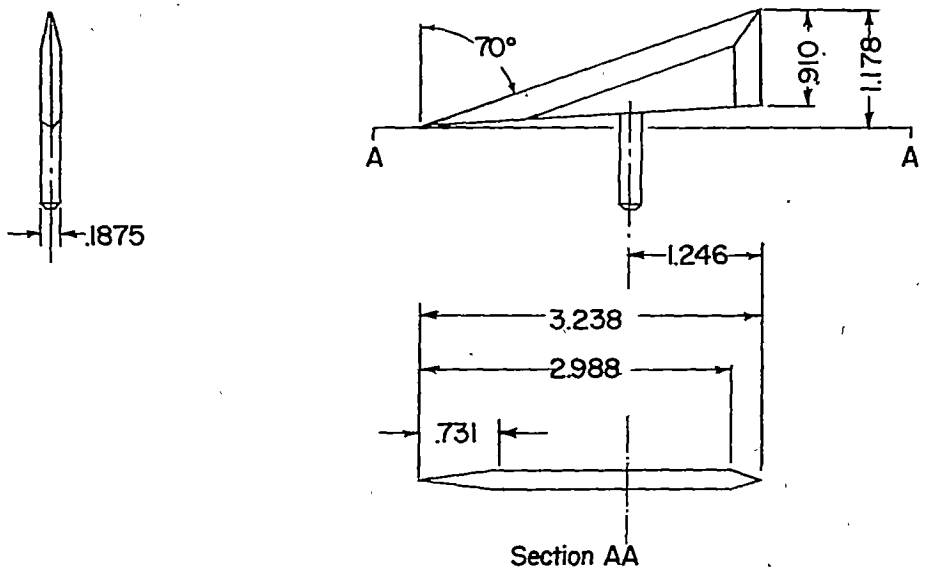

Small vertical canard

All dimensions in inches

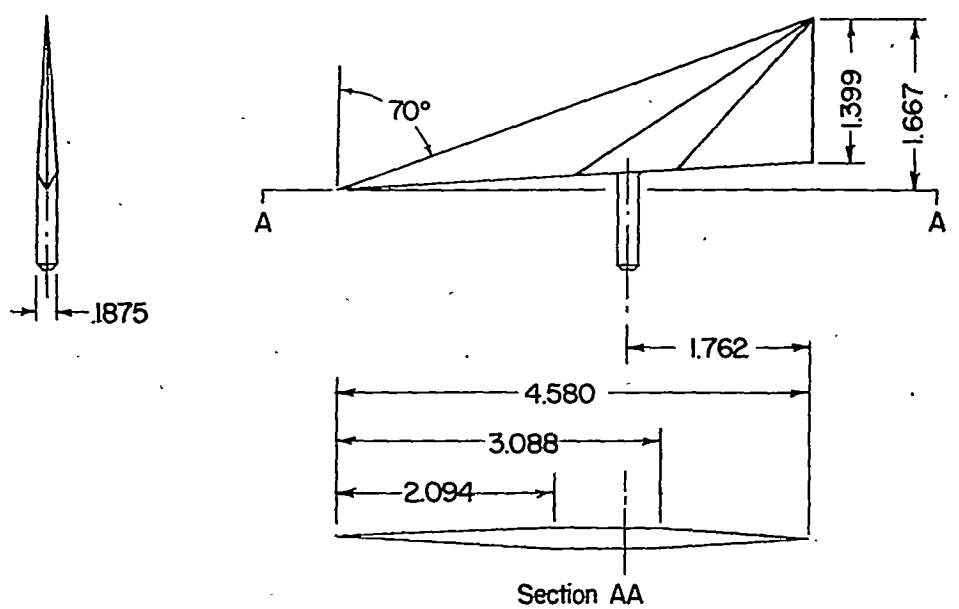

Large vertical and horizontal canard

(a) Canards.

Figure 4.- Control-surface details.

[redacted]

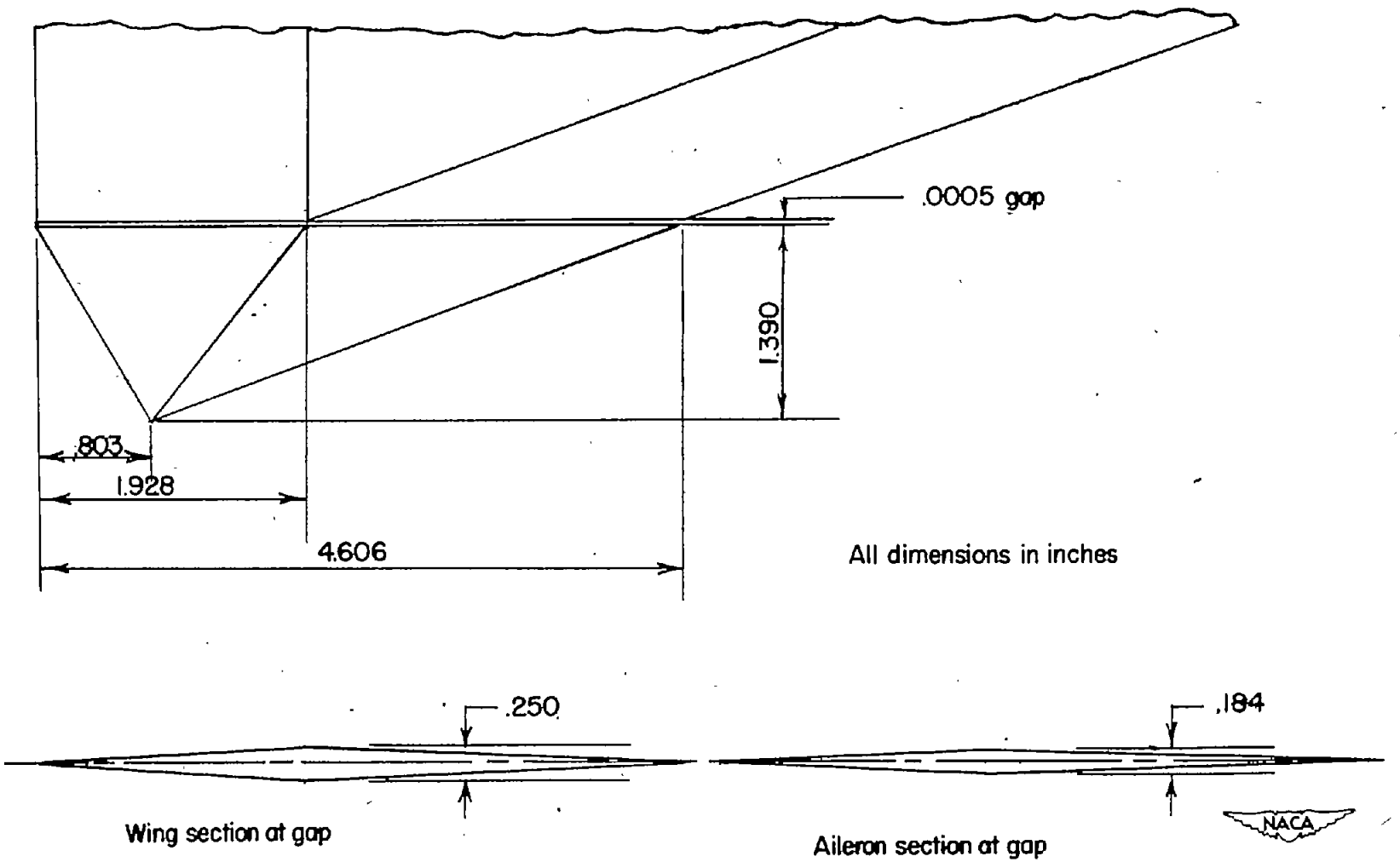

(b) Aileron.

Figure 4.- Concluded.

[redacted]

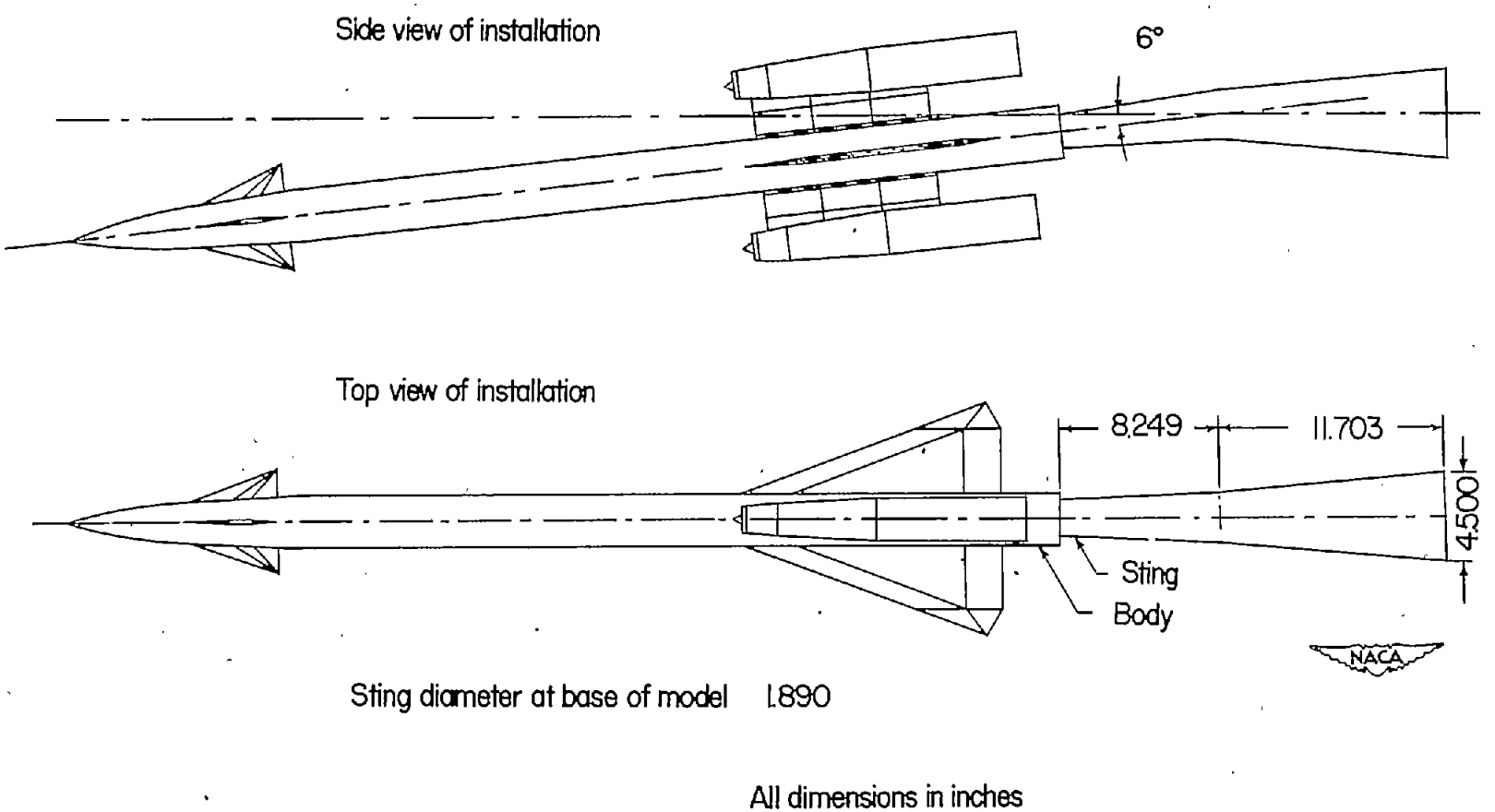

Figure 5.- Details of model installation.

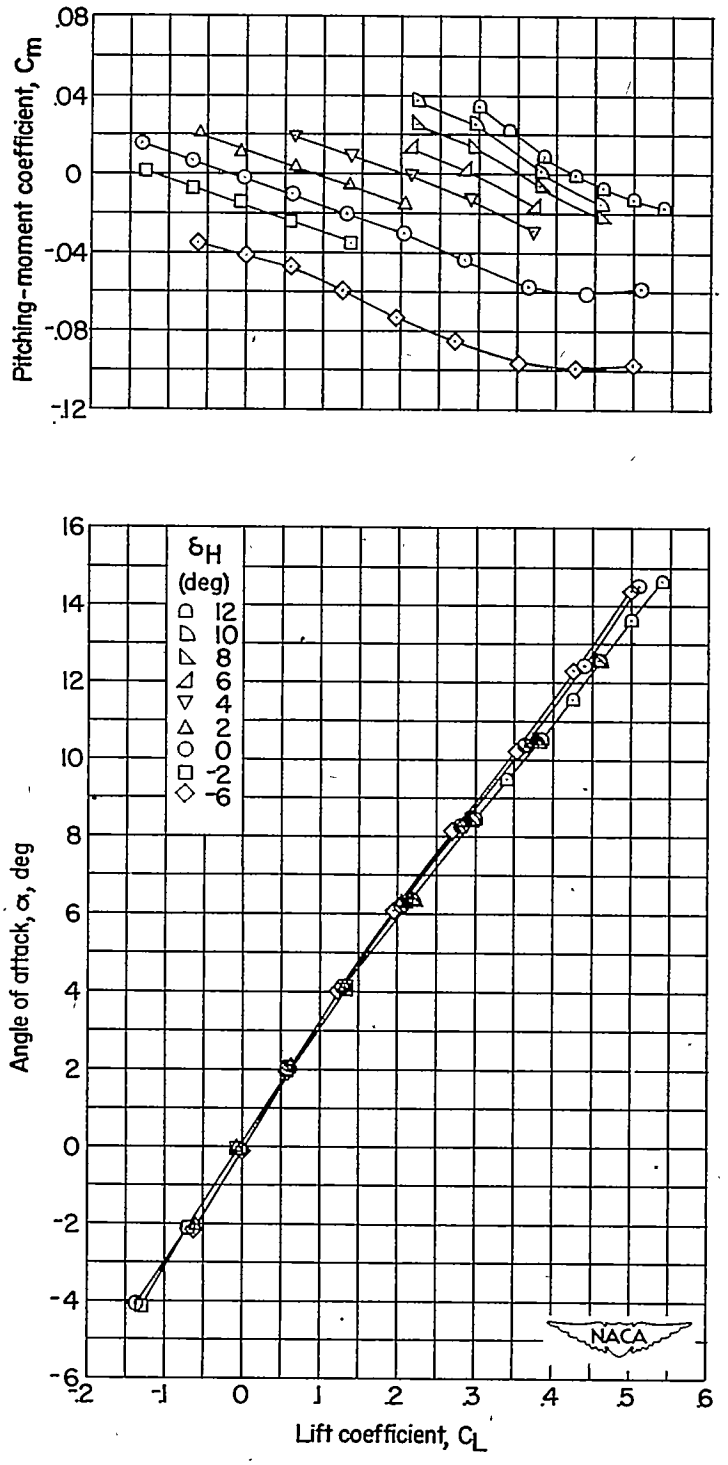

(a) Large vertical canards; forward nacelles.

Figure 6.- Aerodynamic characteristics in pitch of several configurations of a ram-jet missile model with canard surfaces.

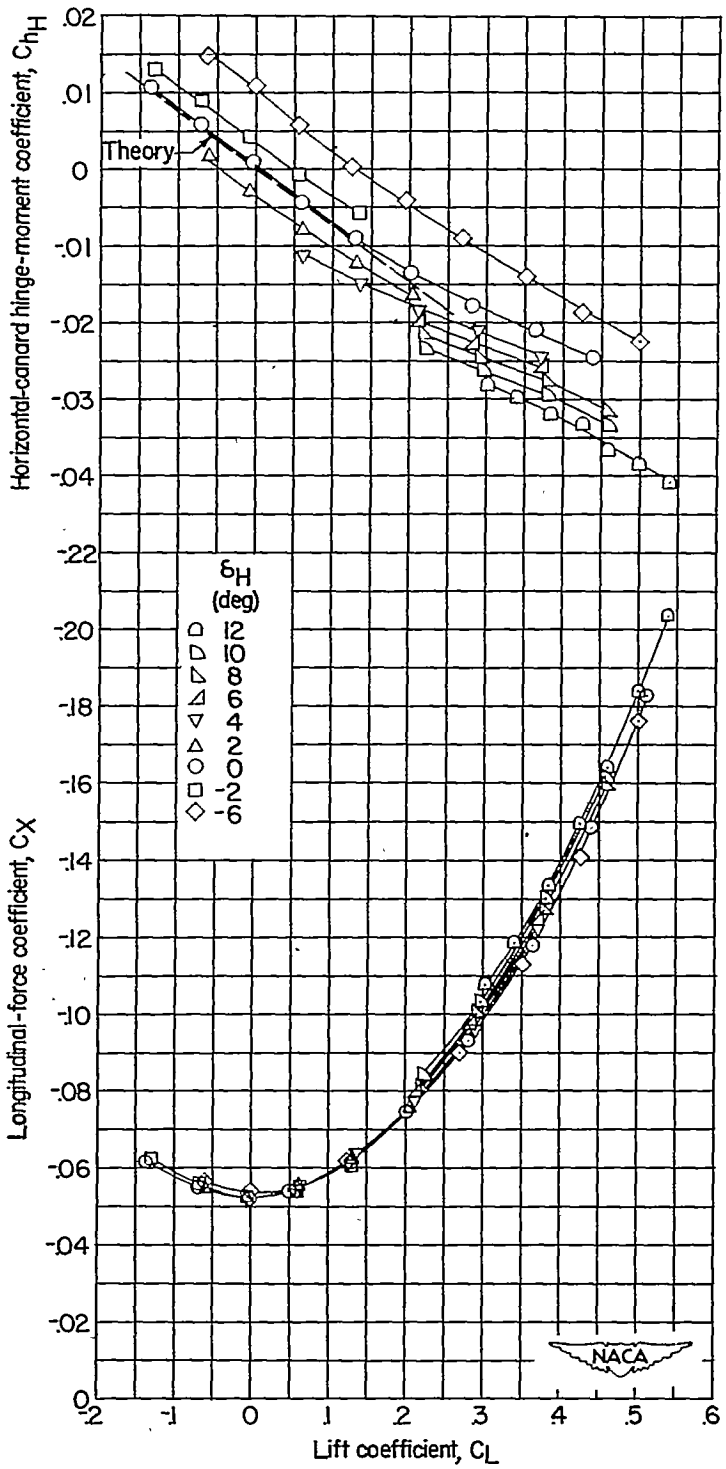

(a) Concluded.

Figure 6.- Continued.

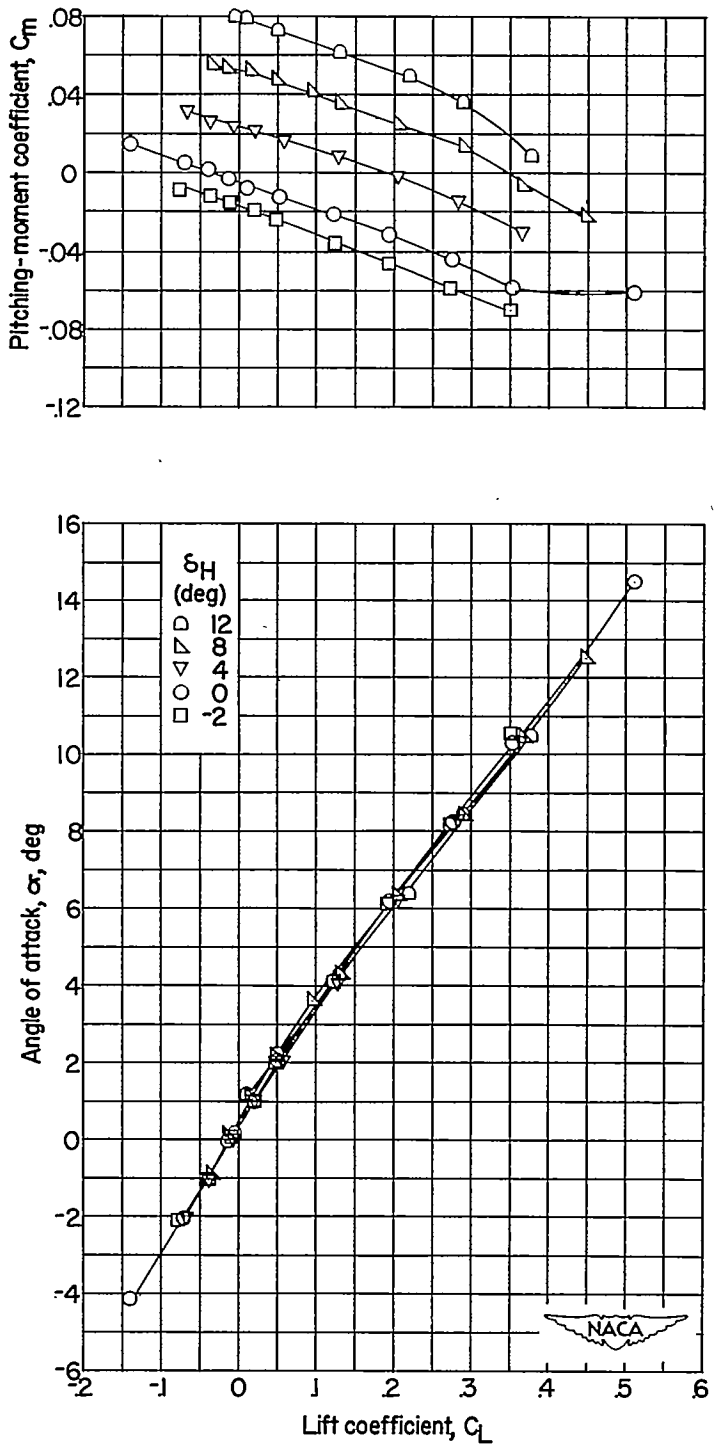

(b) Small vertical canards; forward nacelles.

Figure 6.- Continued.

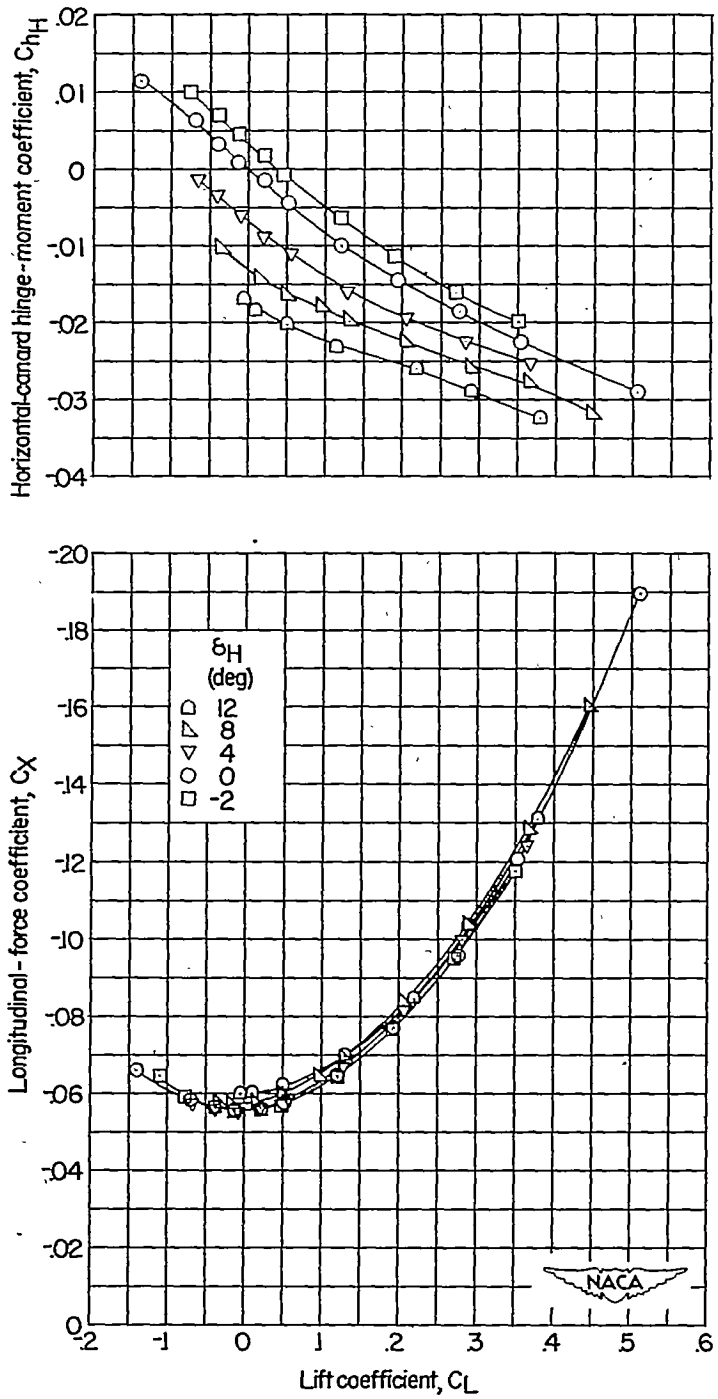

(b) Concluded.

Figure 6.- Continued.

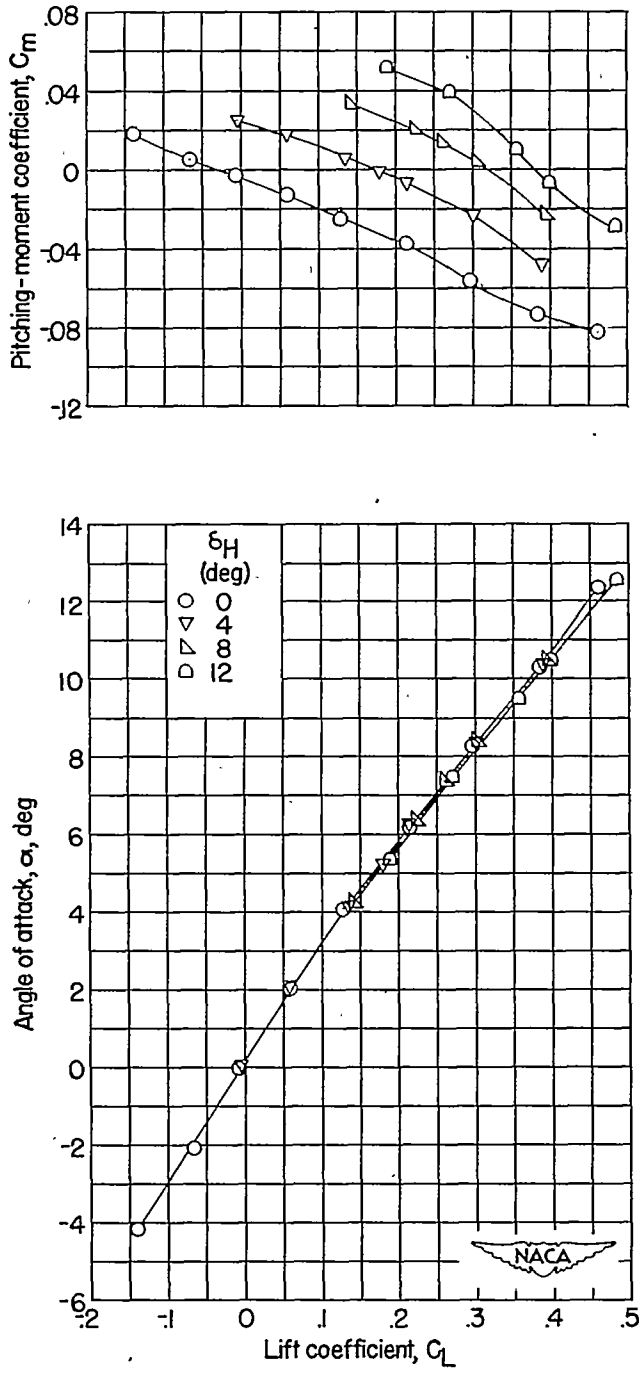

(c) Small vertical canards; rearward nacelle.

Figure 6.- Continued.

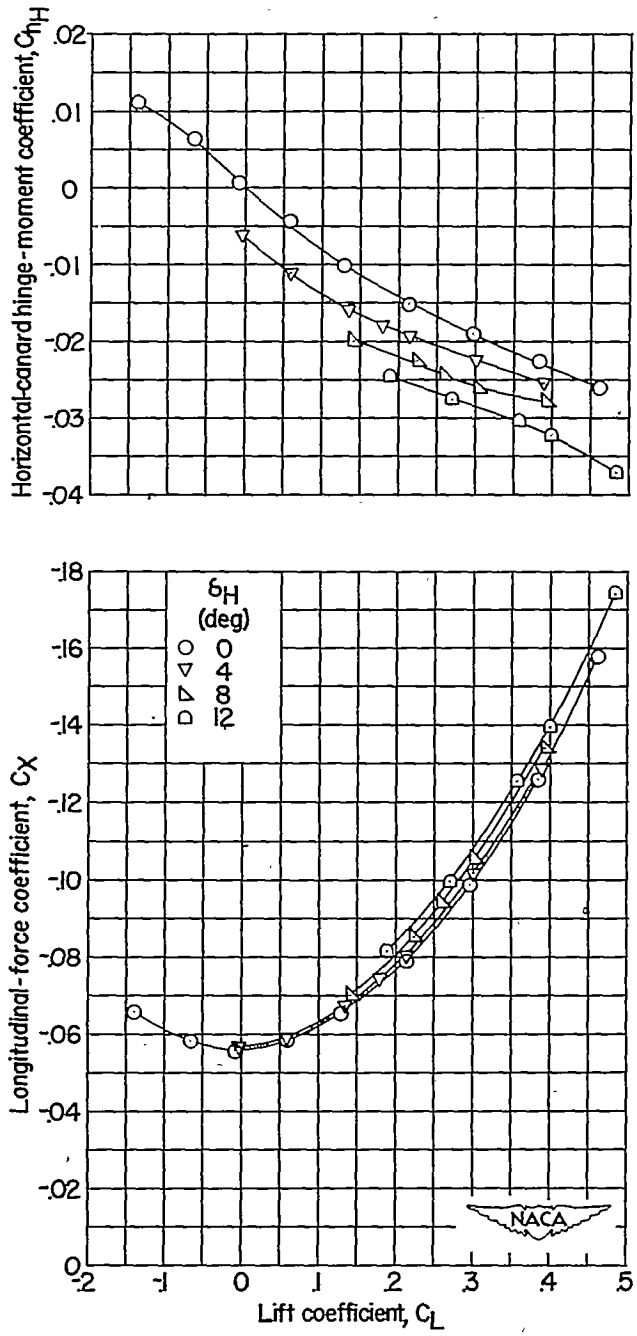

(c) Concluded.

Figure 6.- Concluded.

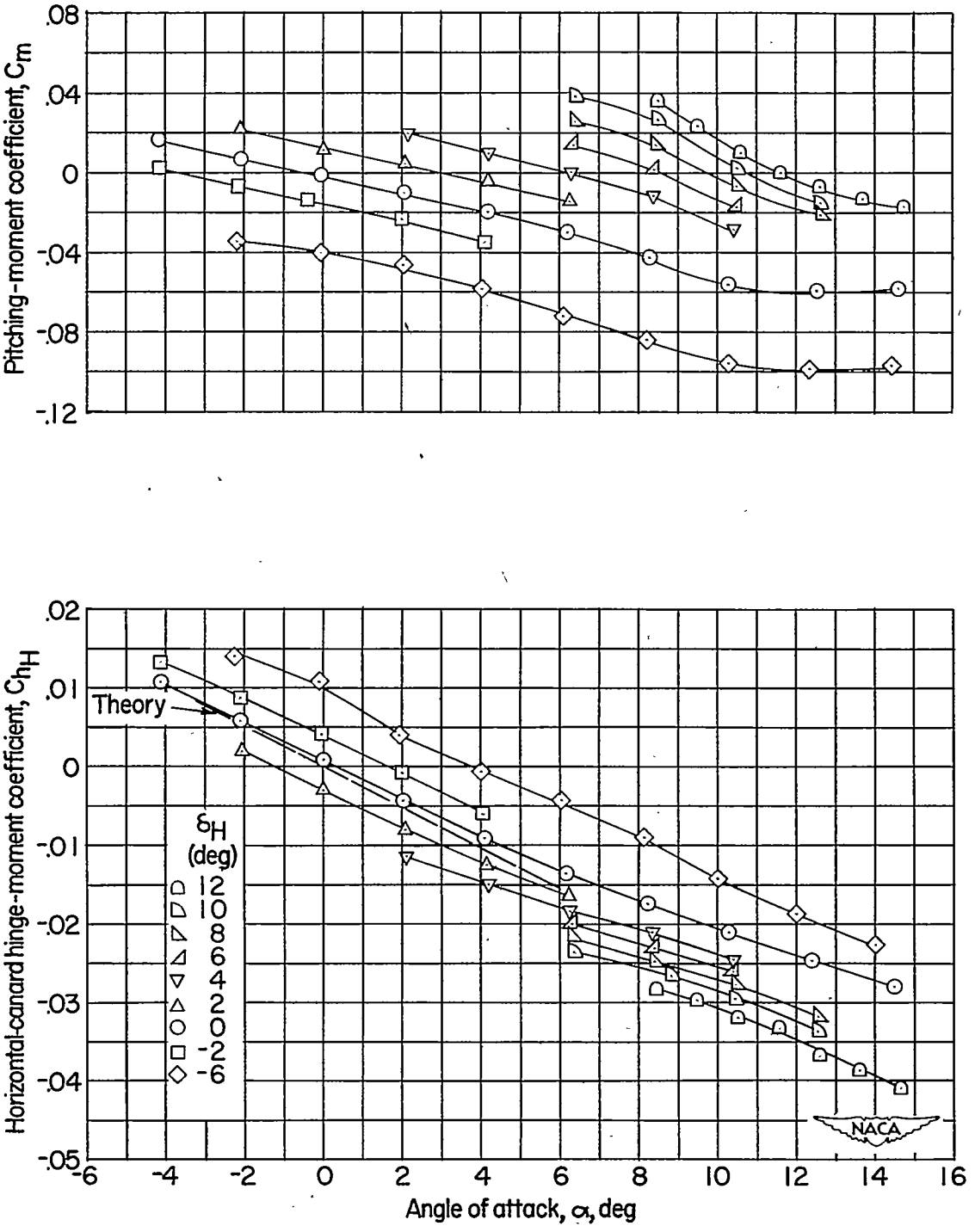

(a) Large vertical canards; forward nacelles.

Figure 7.- Variation of pitching-moment coefficient and horizontal-canard hinge-moment coefficient with angle of attack for various horizontal-canard deflections.

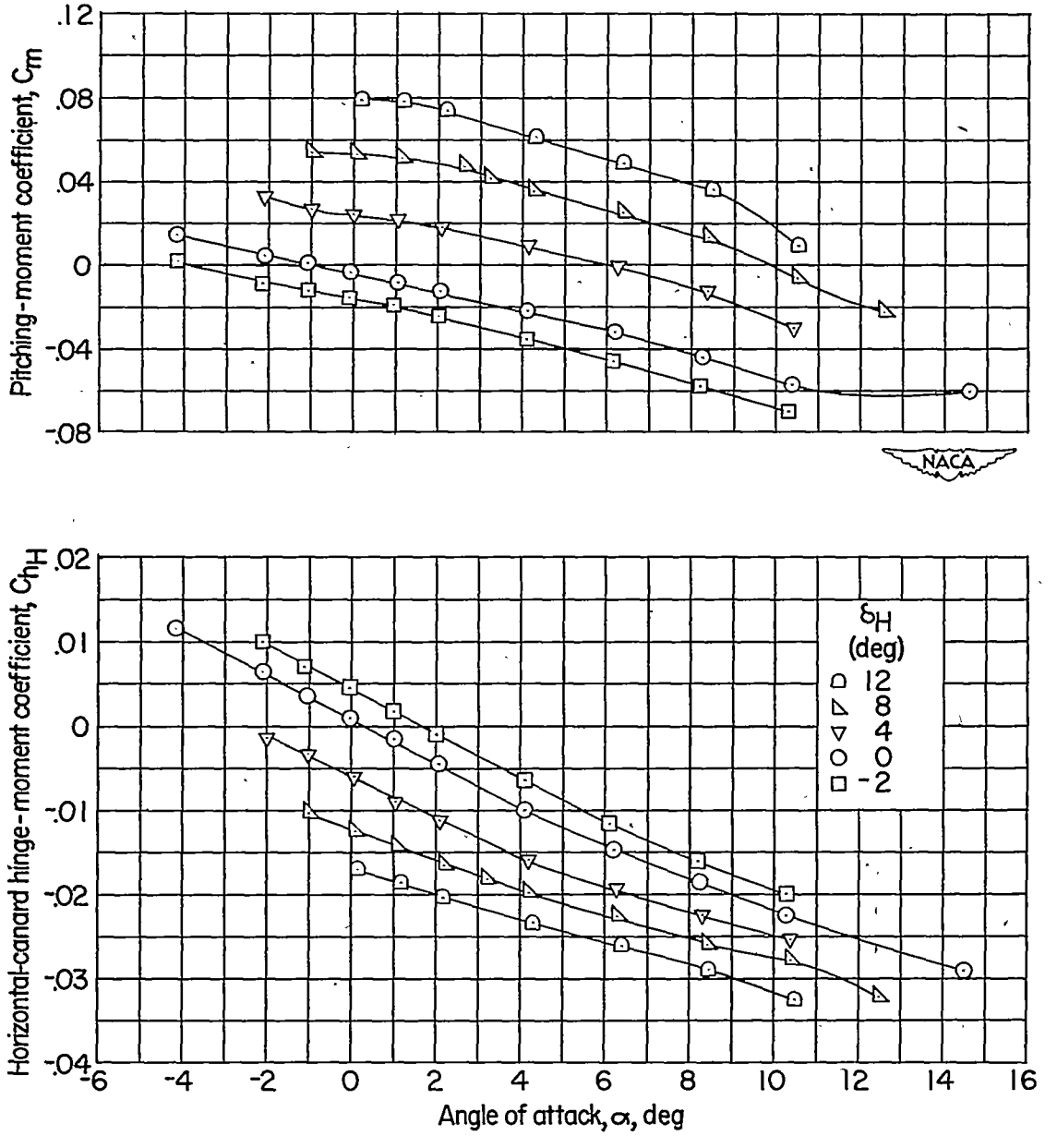

(b) Small vertical canard; forward nacelles.

Figure 7.- Continued.

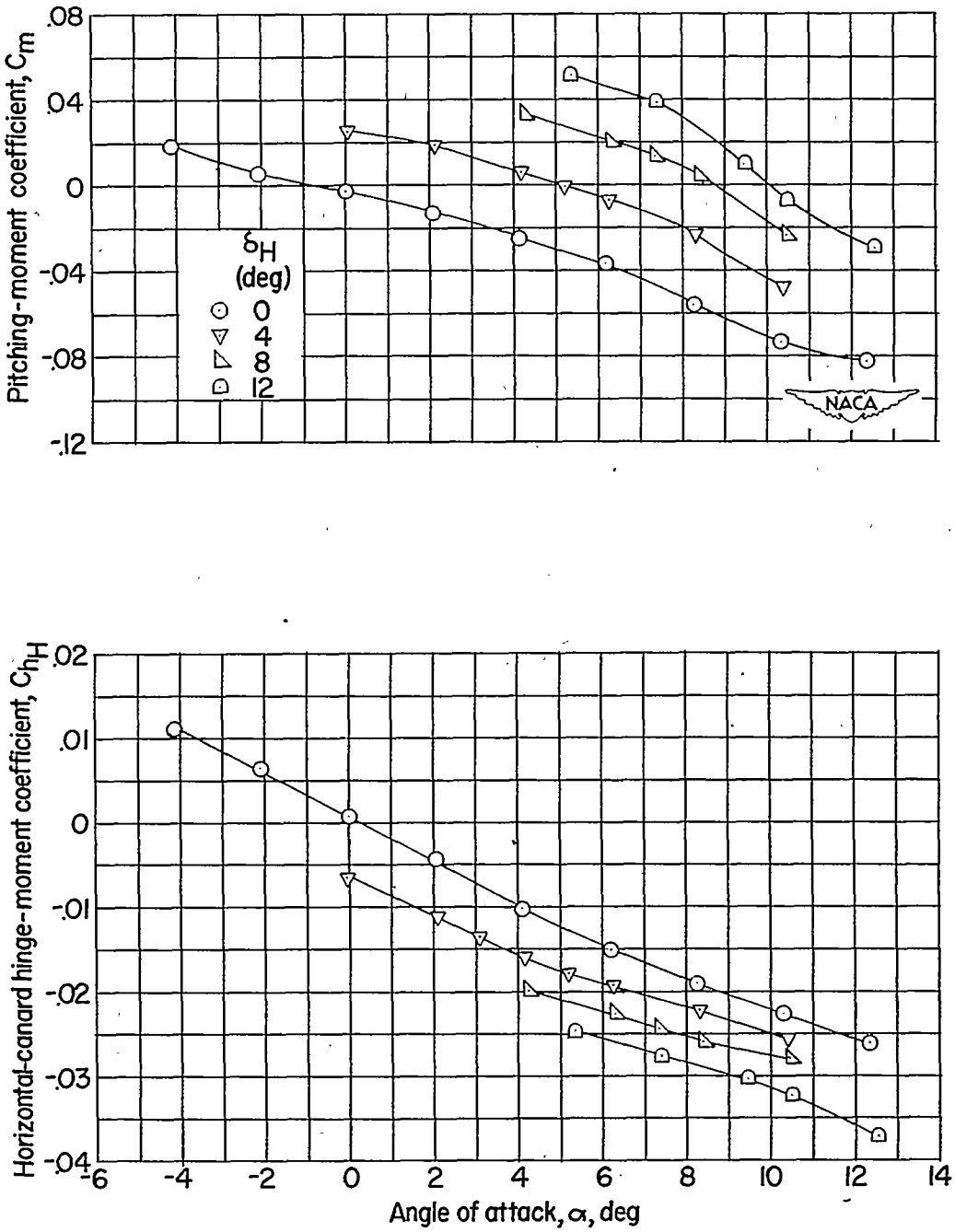

(c) Small vertical canards; rearward nacelles.

Figure 7.- Concluded.

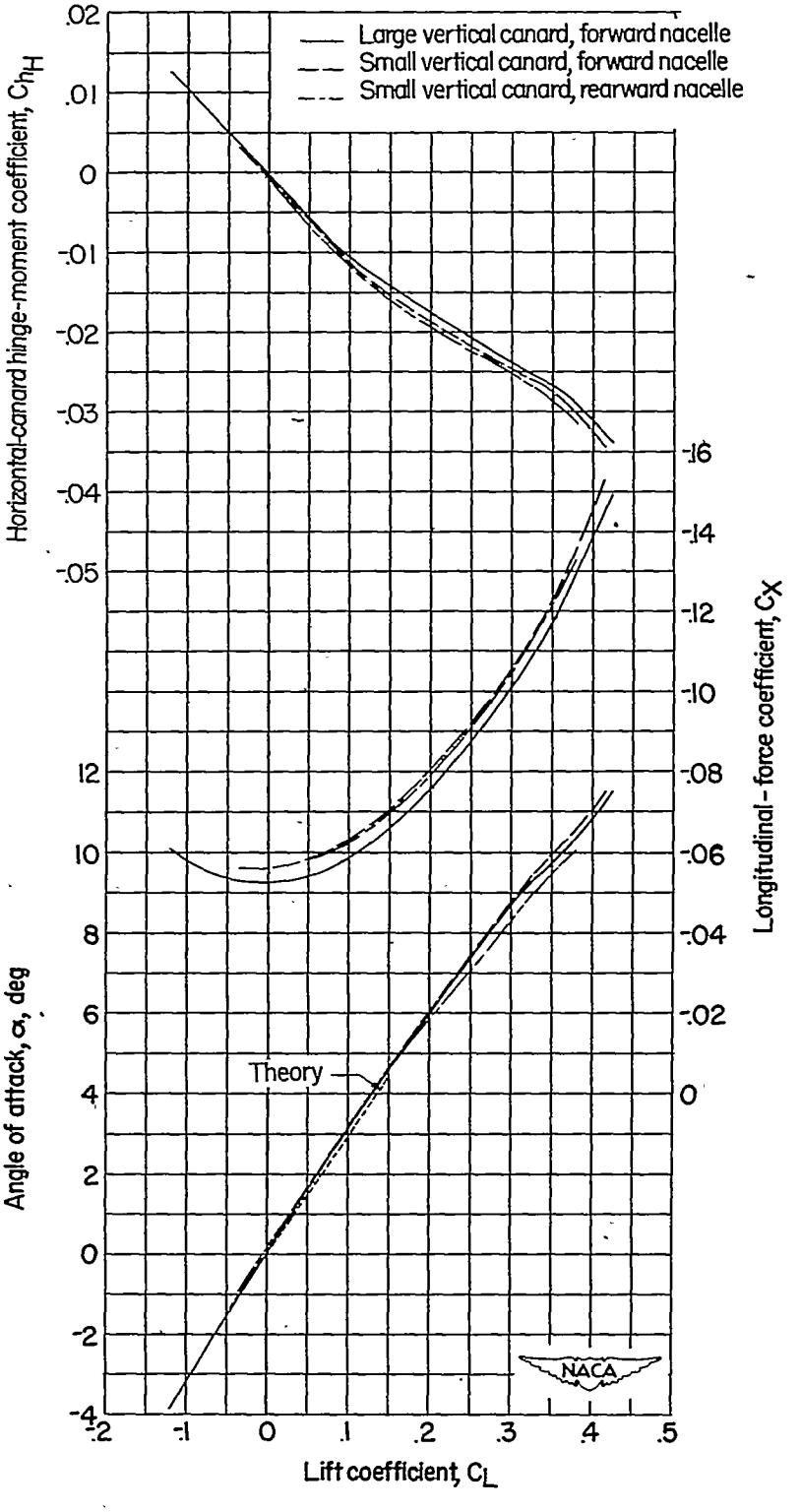

Figure 8.- Longitudinal characteristics for trim ($C_m = 0$).

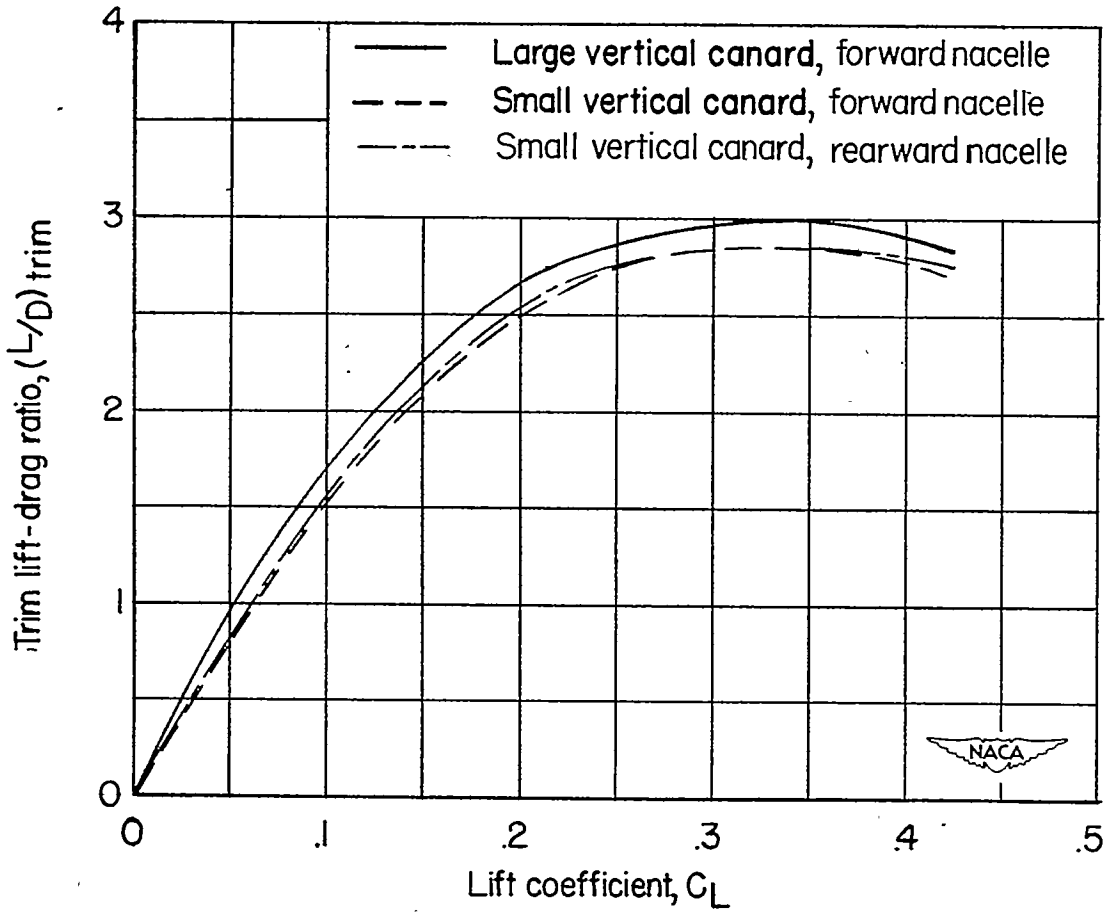

Figure 9.- Variation of trim lift-drag ratio with lift coefficient for the various configurations.

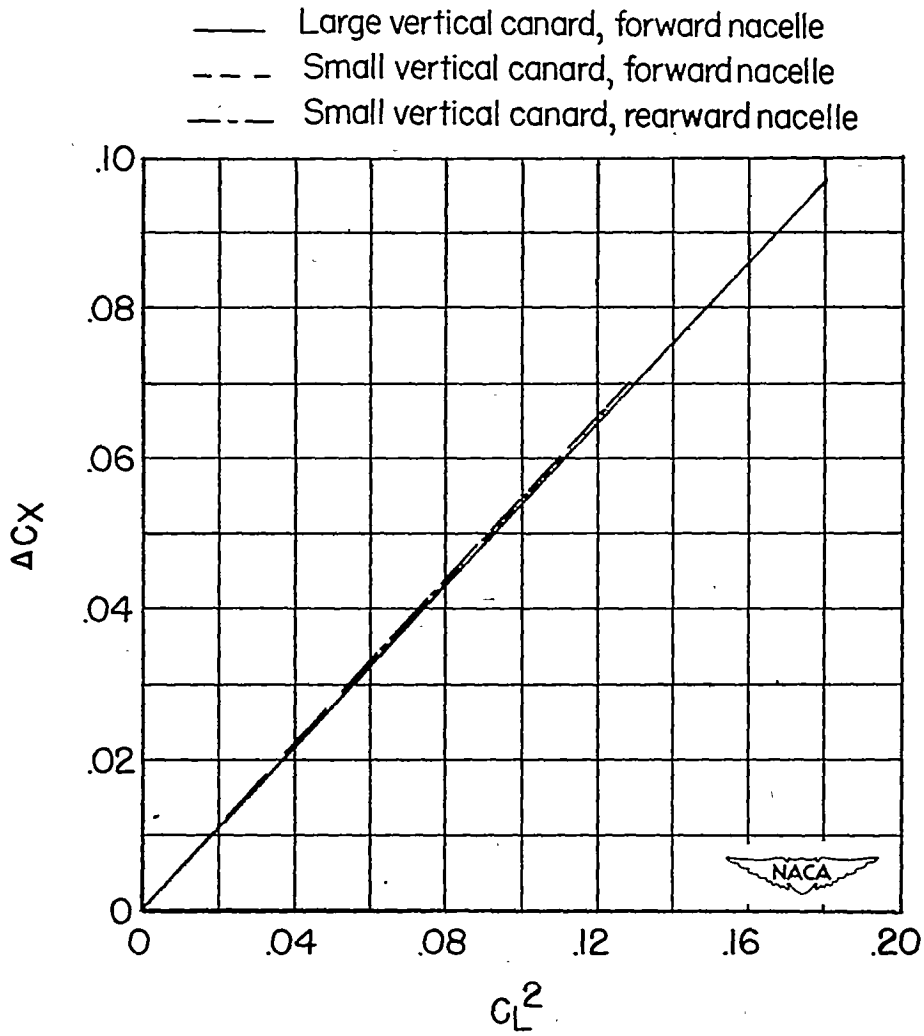

Figure 10.- Drag due to lift.

[redacted]

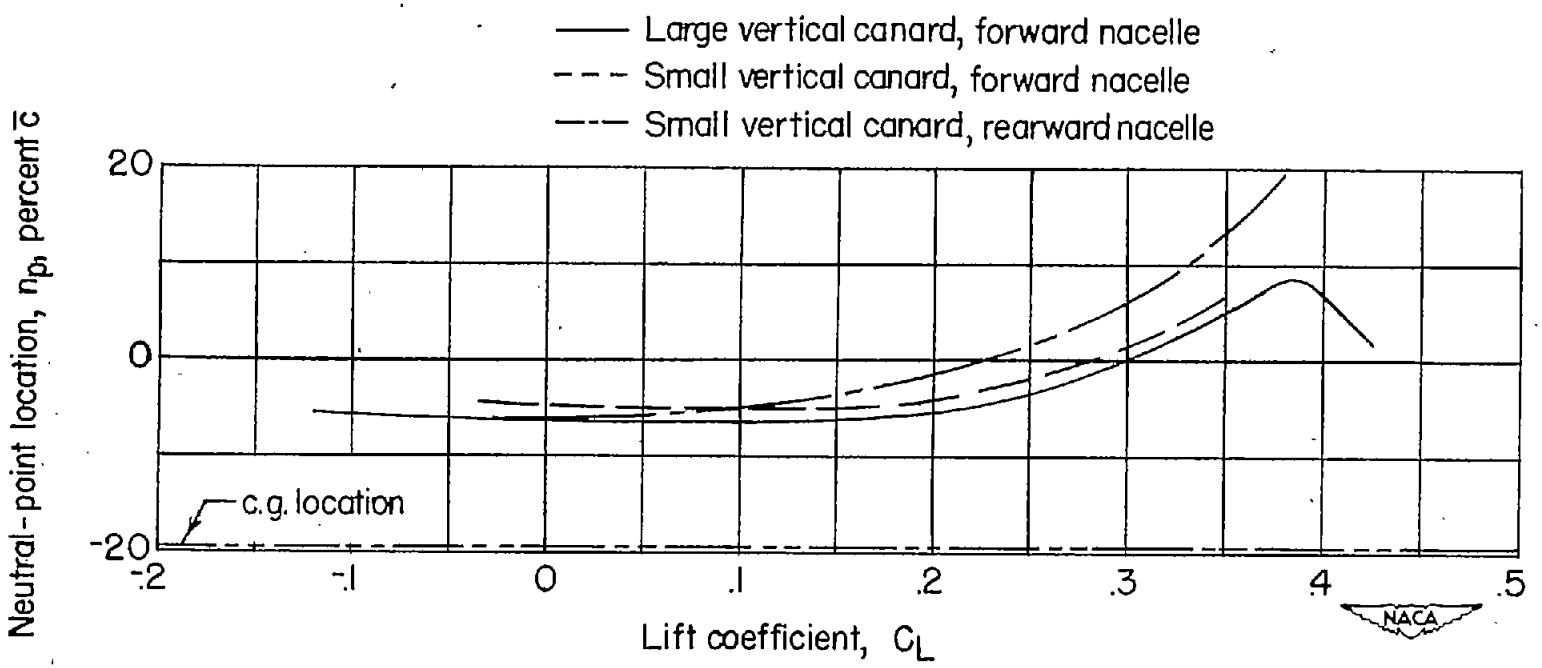

Figure 11.- Variation of neutral point location with lift coefficient for the various configurations.

[redacted]

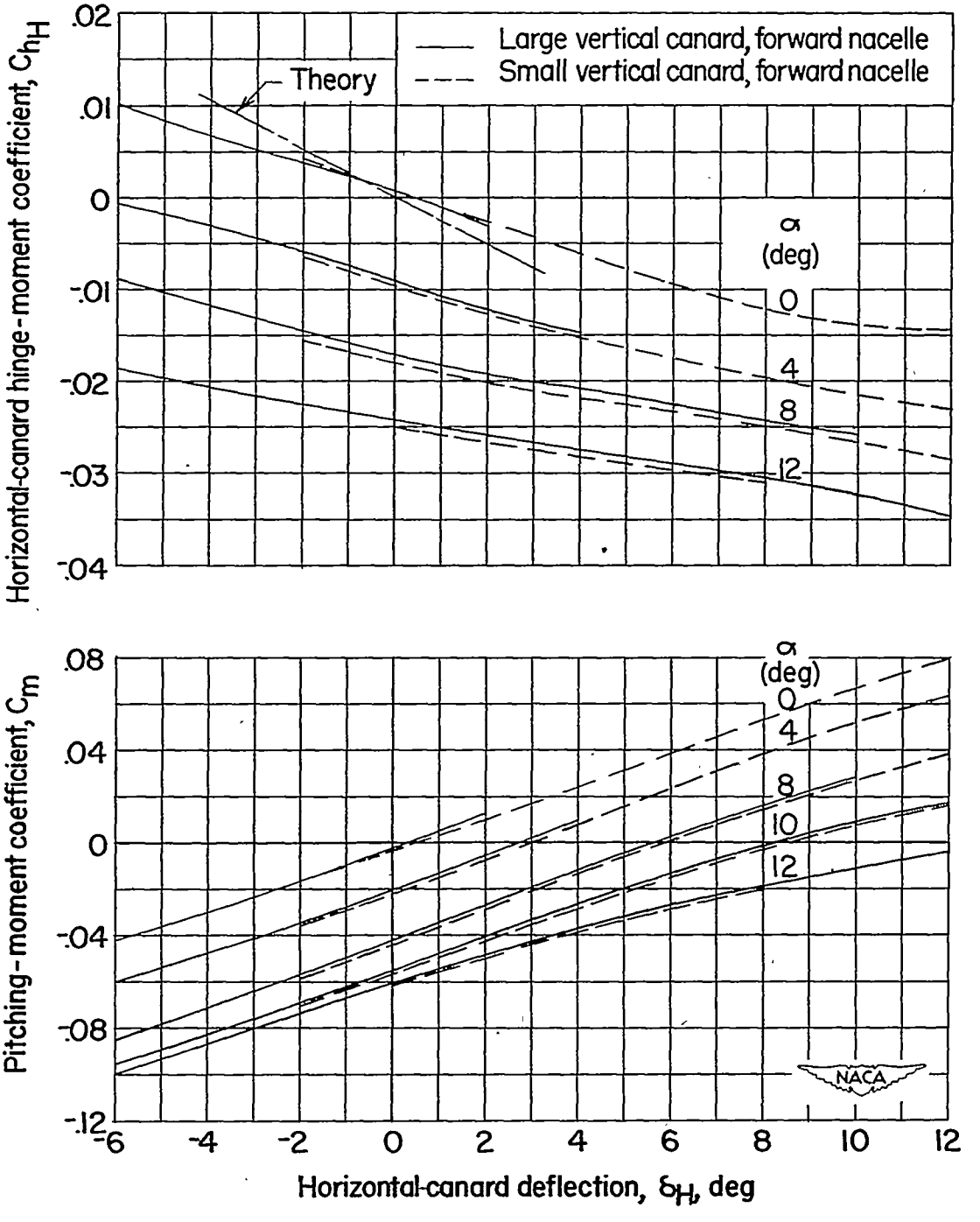

(a) Forward nacelles.

Figure 12.- Variation of pitching-moment coefficient and horizontal-canard hinge-moment coefficient with horizontal-canard deflection for several angles of attack.

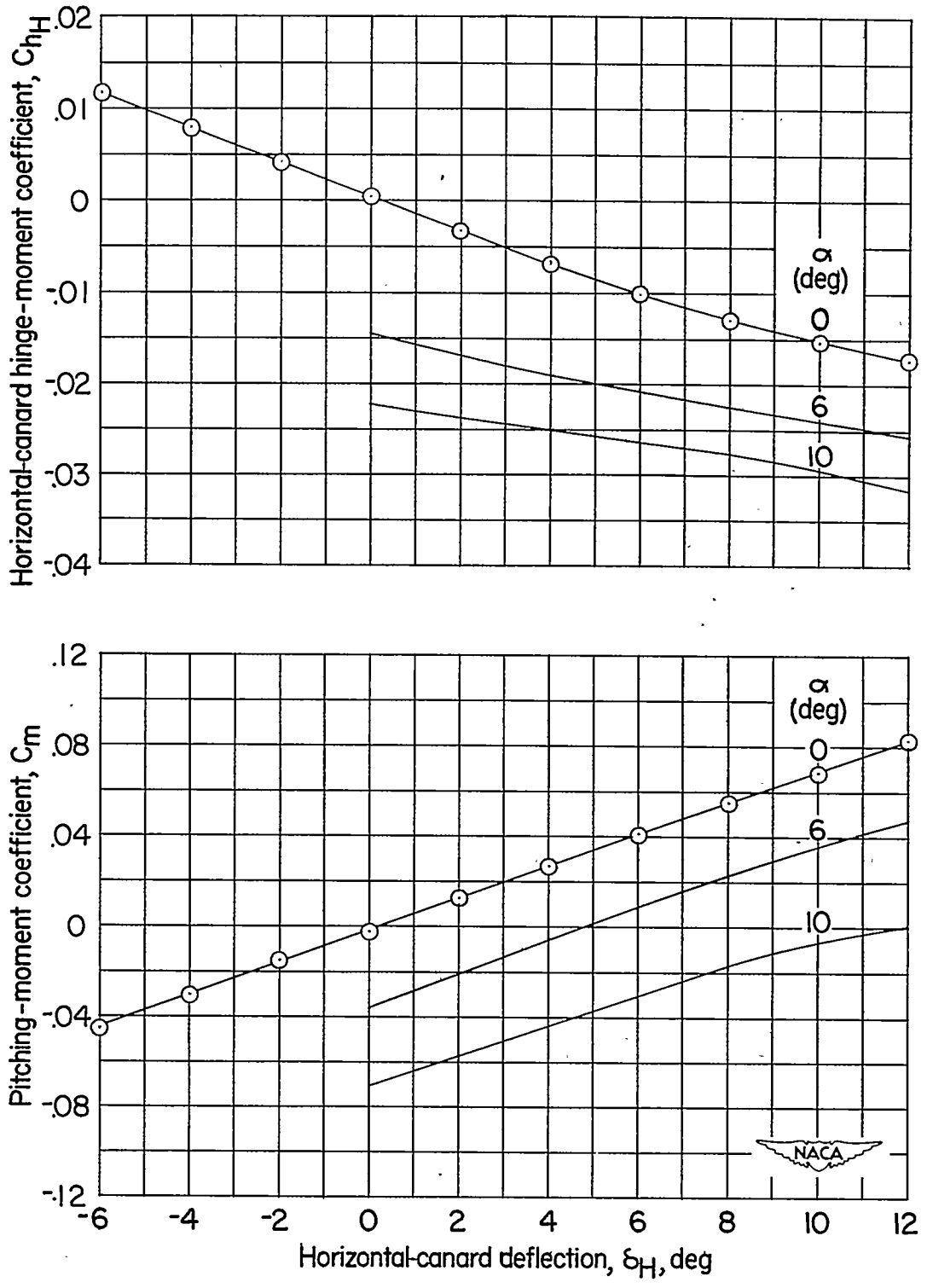

(b) Rearward nacelles.

Figure 12.- Concluded.

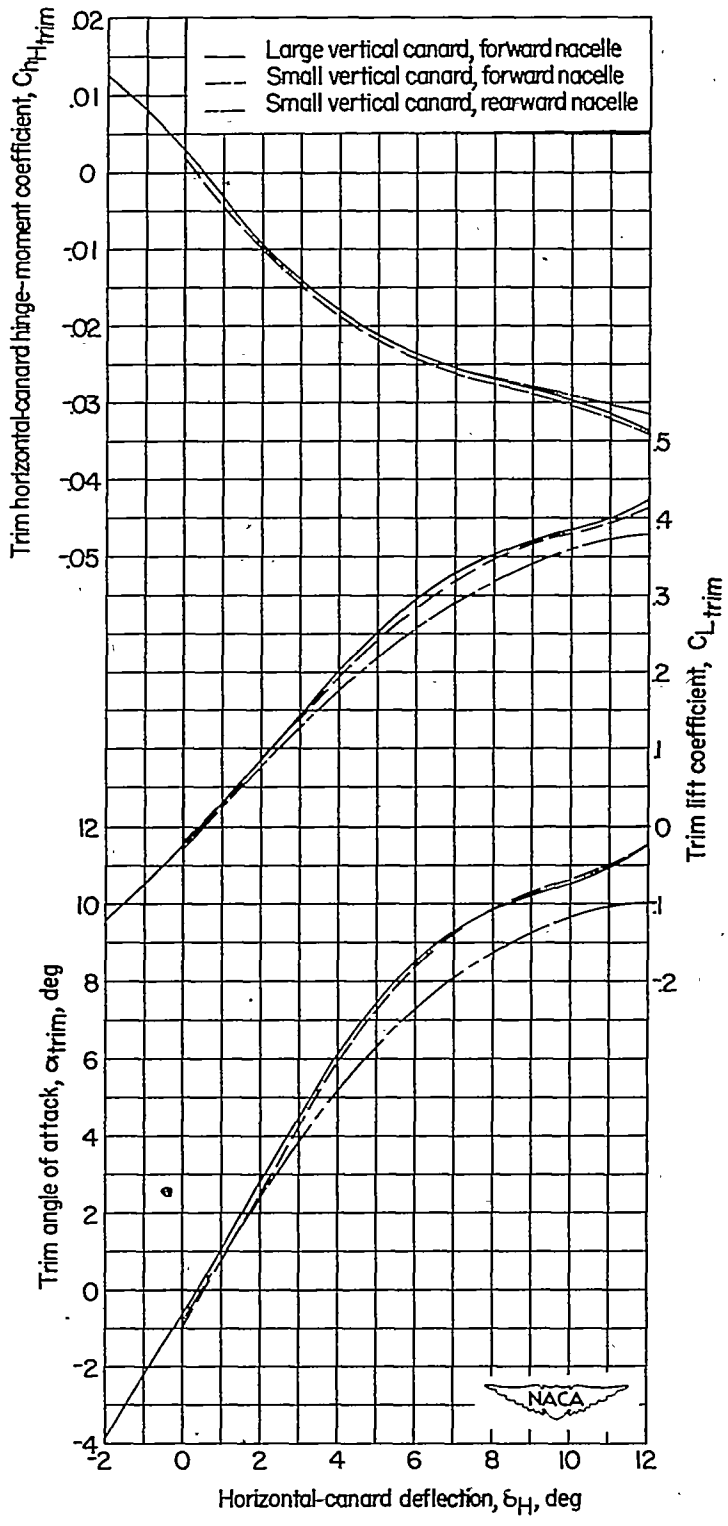

Figure 13.- Variation of trim longitudinal characteristics with horizontal-canard deflection.

[redacted]

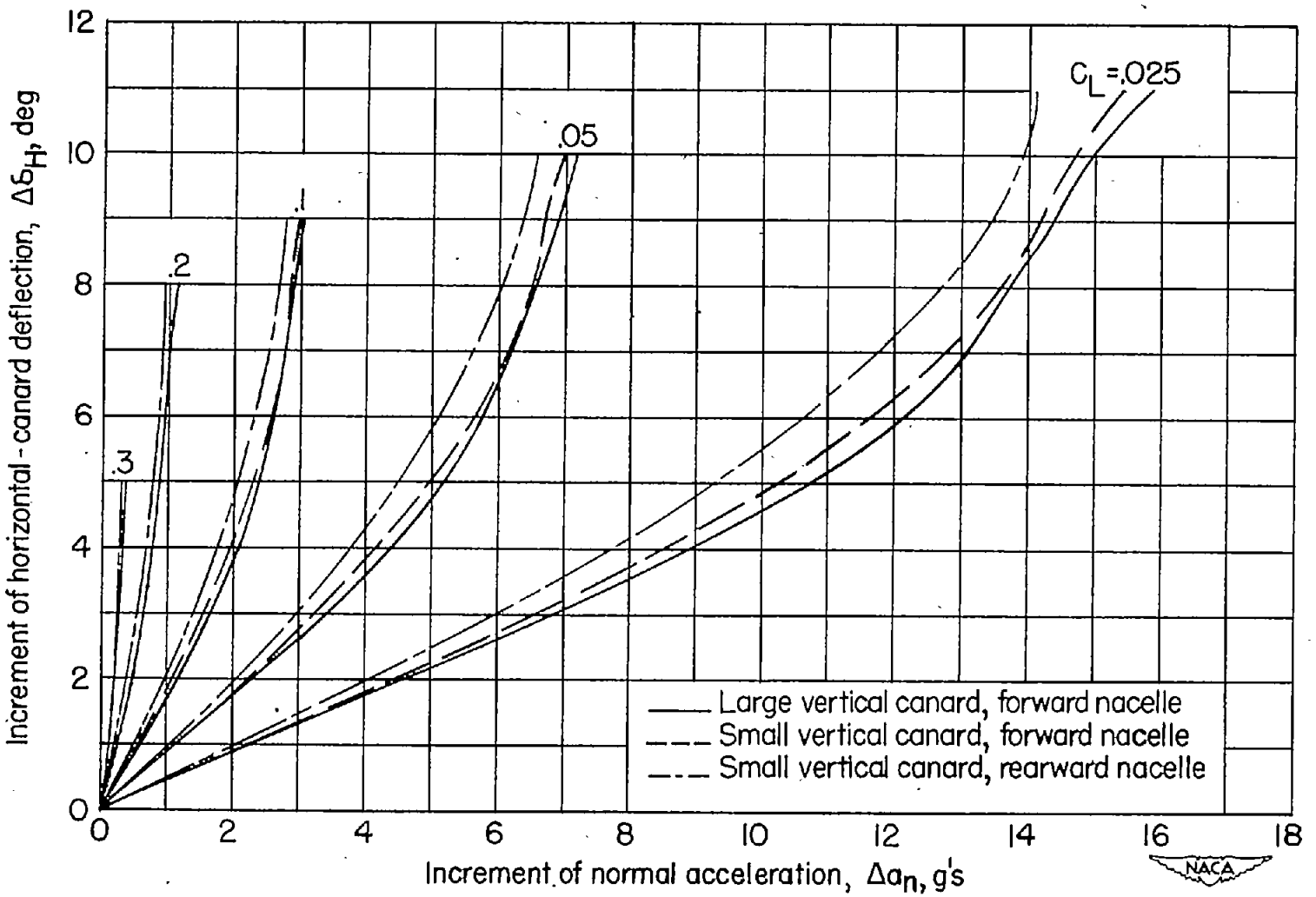

Figure 14.- Variation of normal acceleration with horizontal-canard deflection.

[redacted]

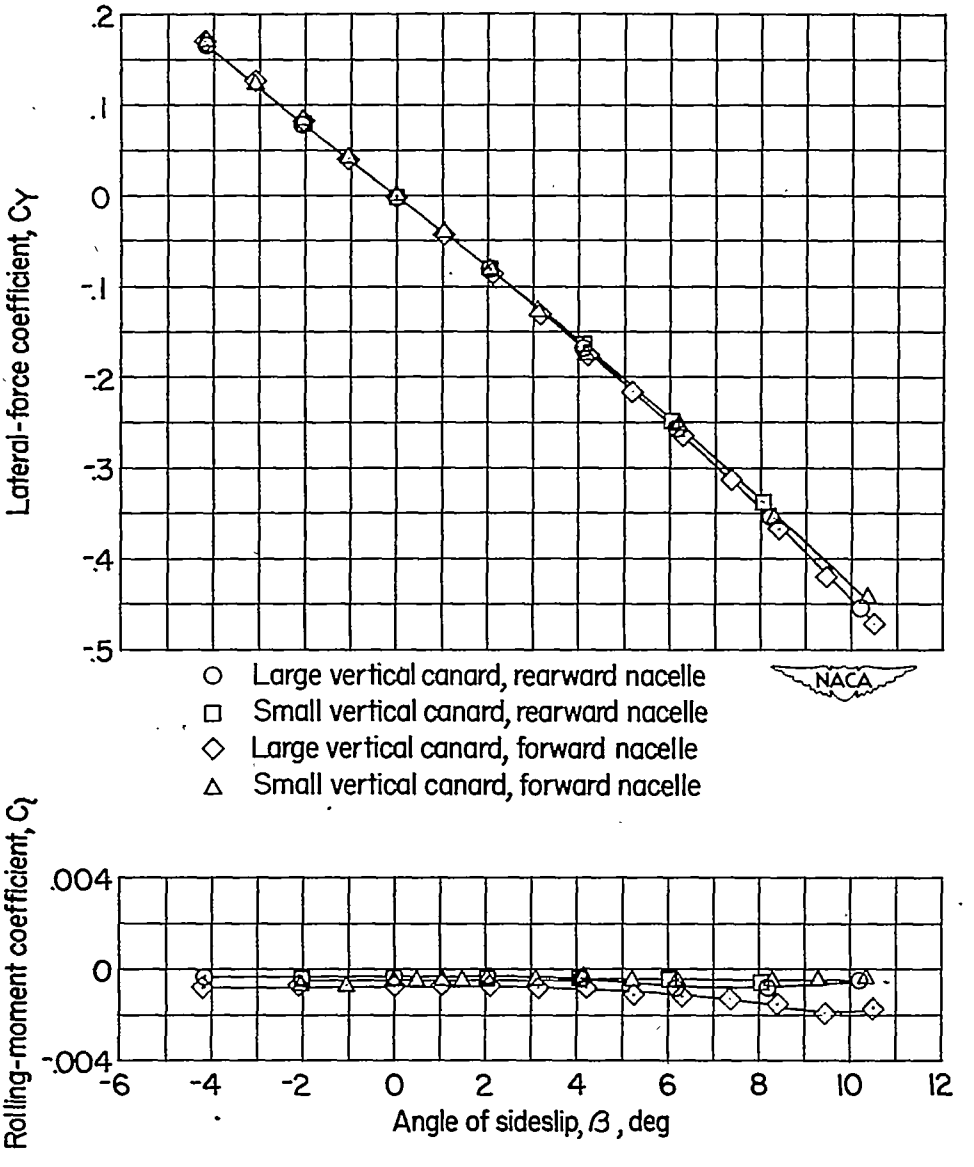

Figure 15.- Aerodynamic characteristics in sideslip for the various configurations. $\alpha = 0^{\circ}$.

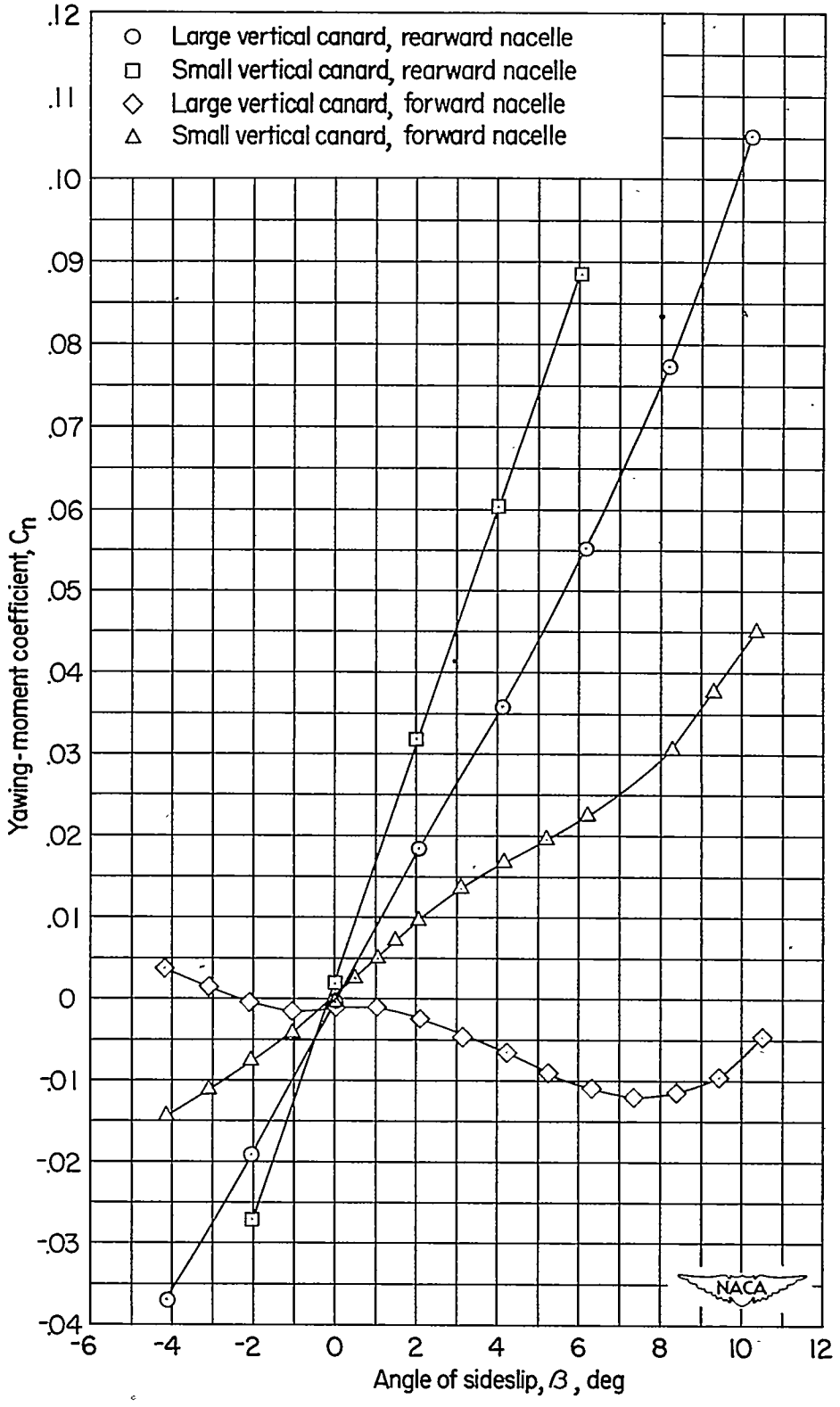

Figure 15.- Concluded.

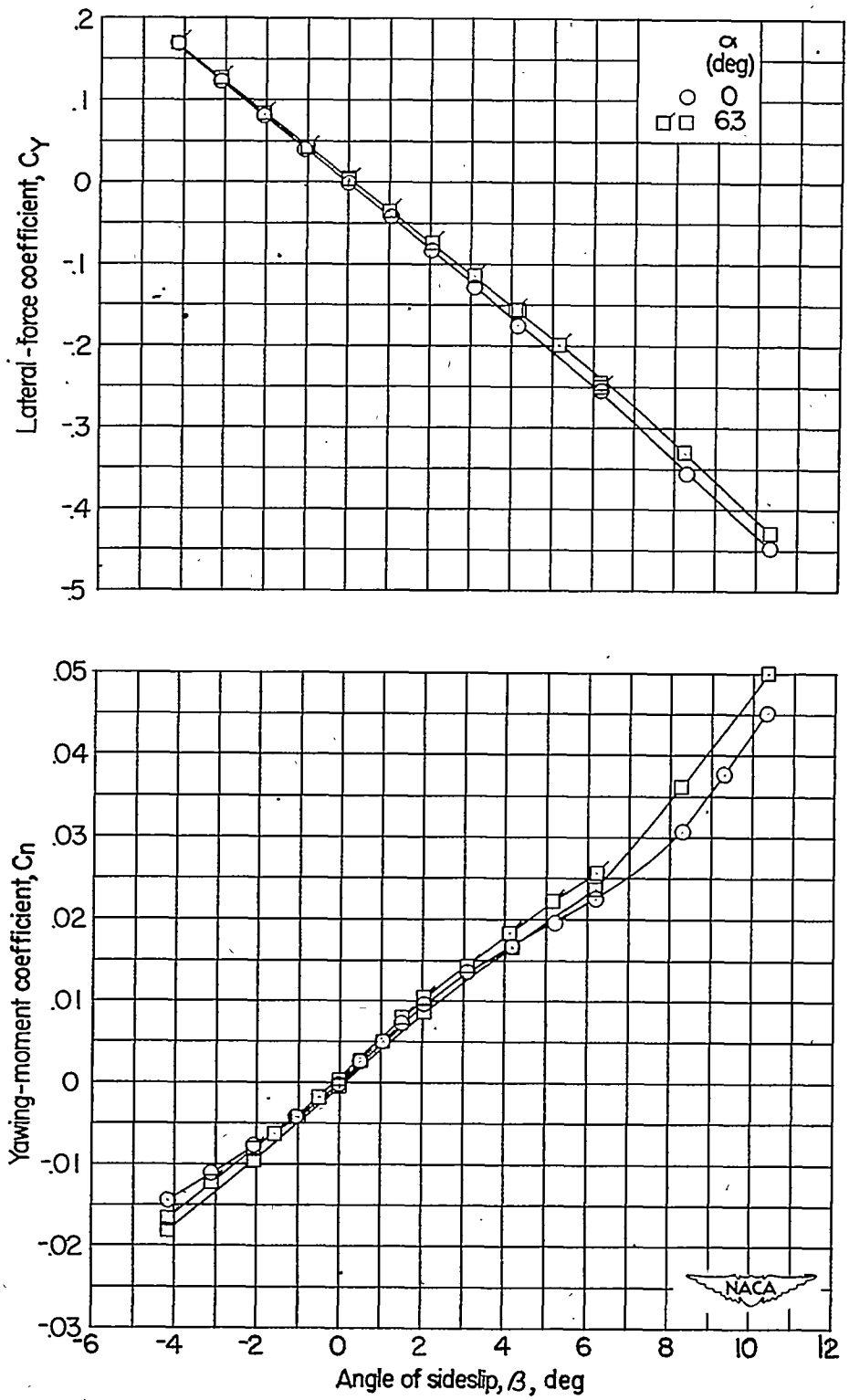

Figure 16.- Effect of angle of attack on the aerodynamic characteristics in sideslip. Small vertical canard; forward nacelle location.

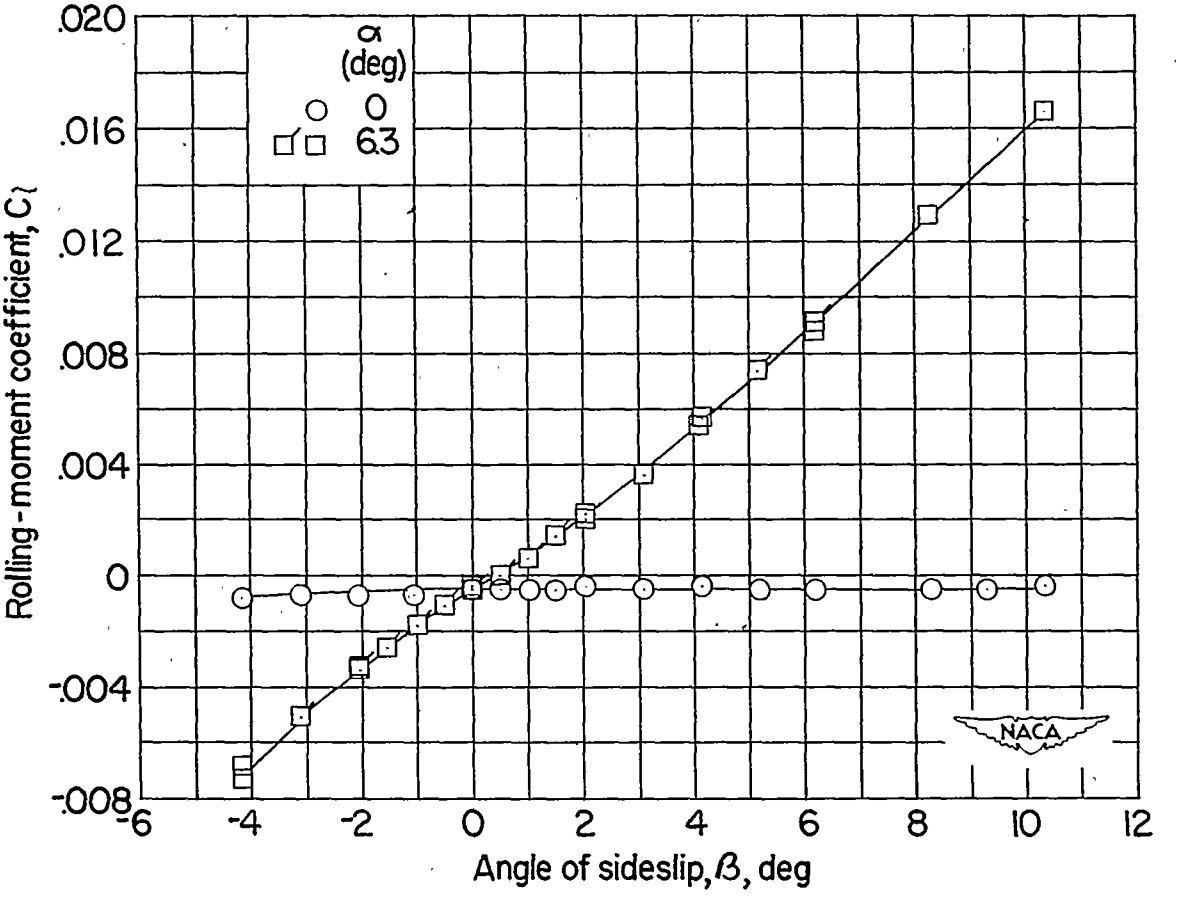

Figure 16.- Continued.

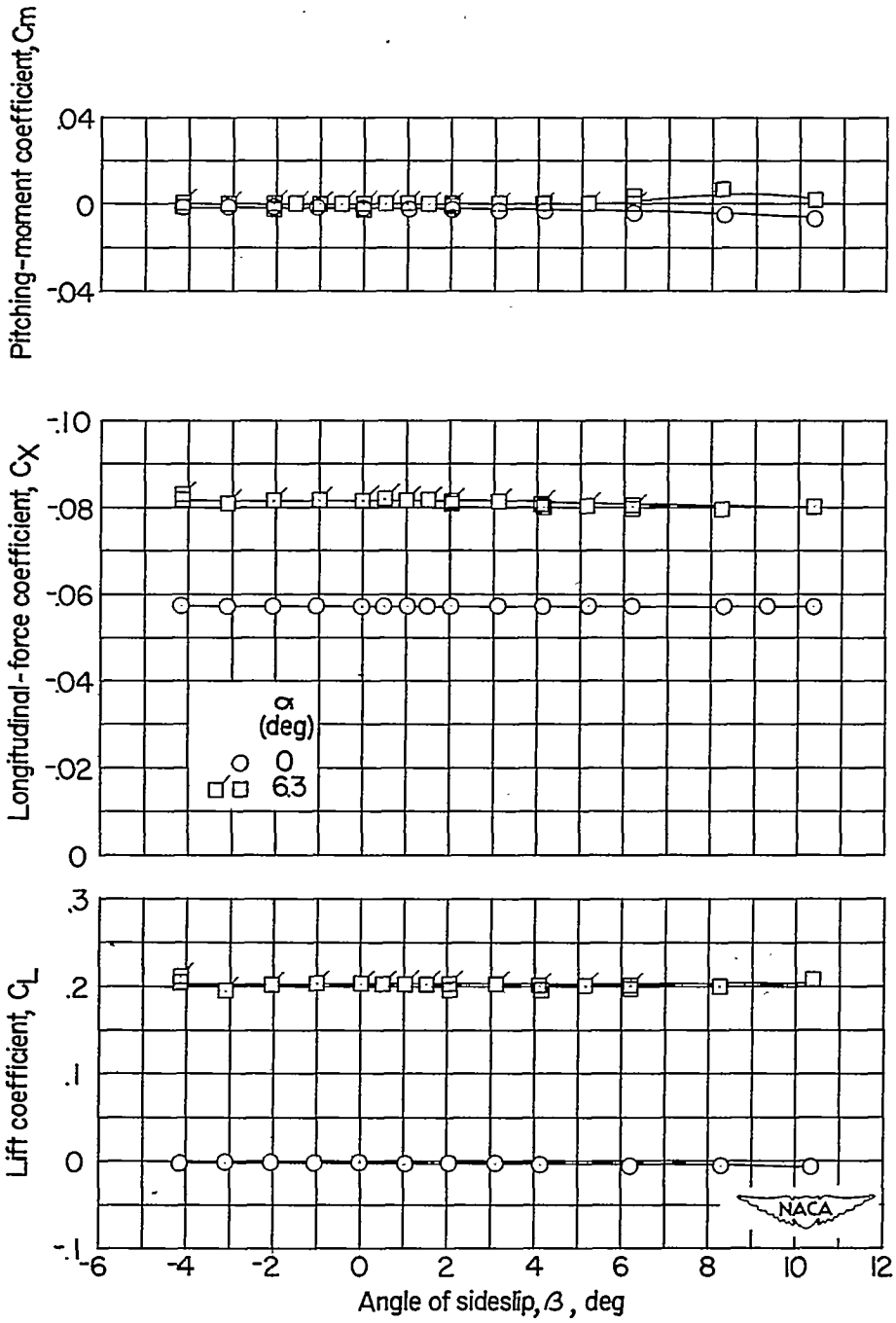

Figure 16.- Concluded.

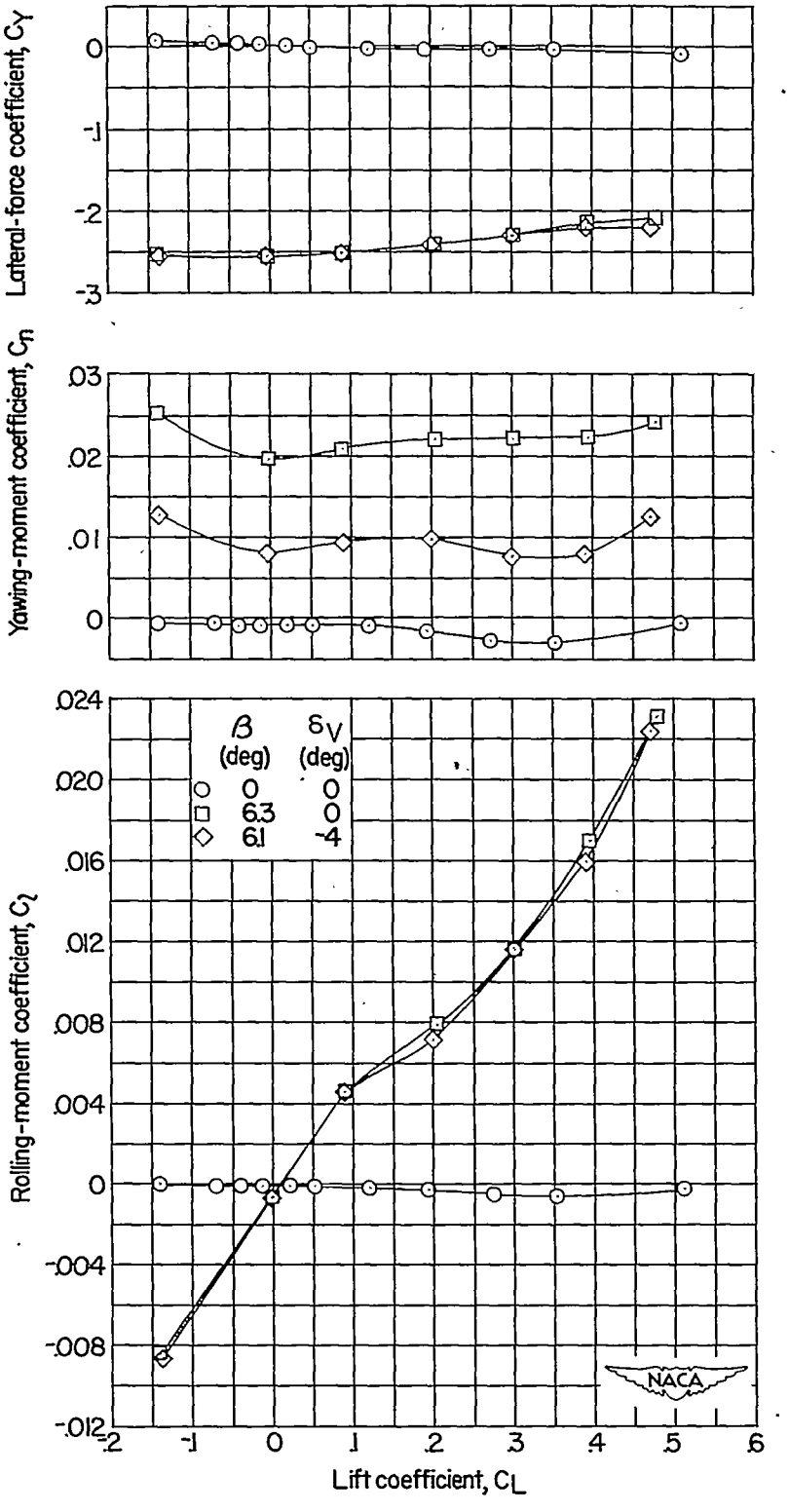

Figure 17.- Variation of lateral characteristics with lift coefficient. Small vertical canard; forward nacelle location.

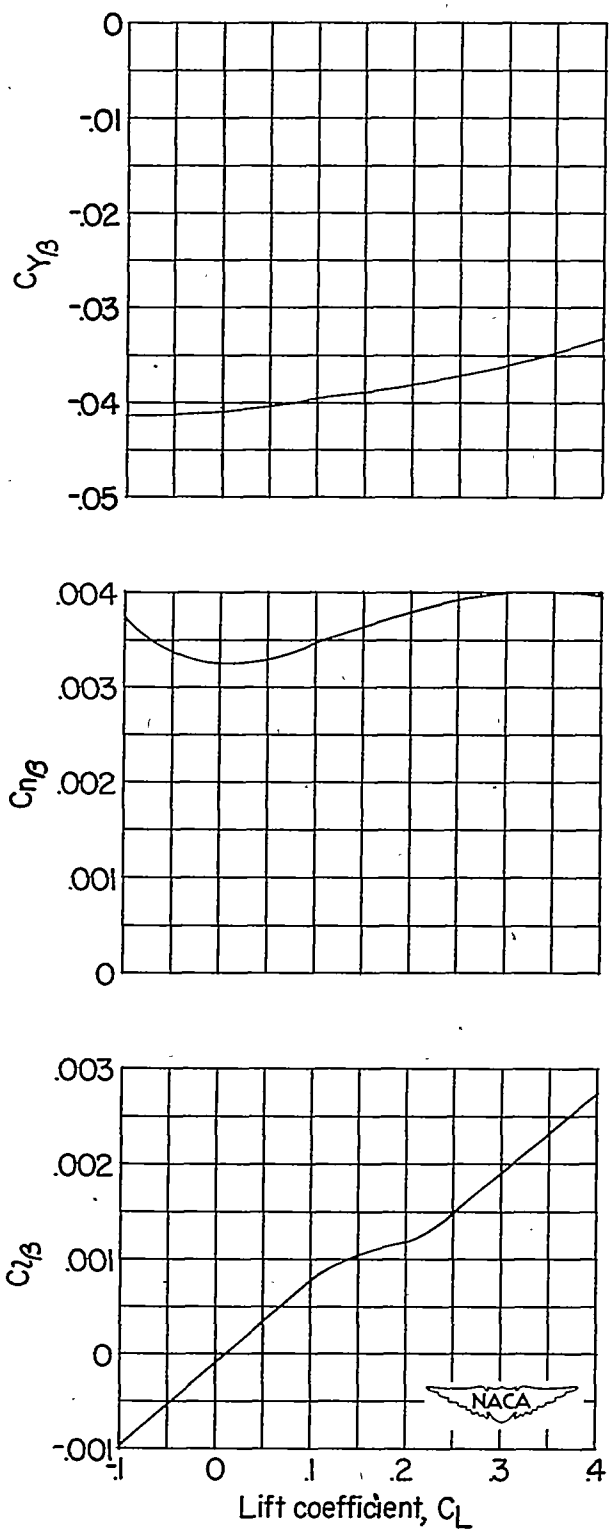

Figure 18.- Variation of the sideslip derivatives with lift coefficient. Small vertical canard; forward nacelle location.

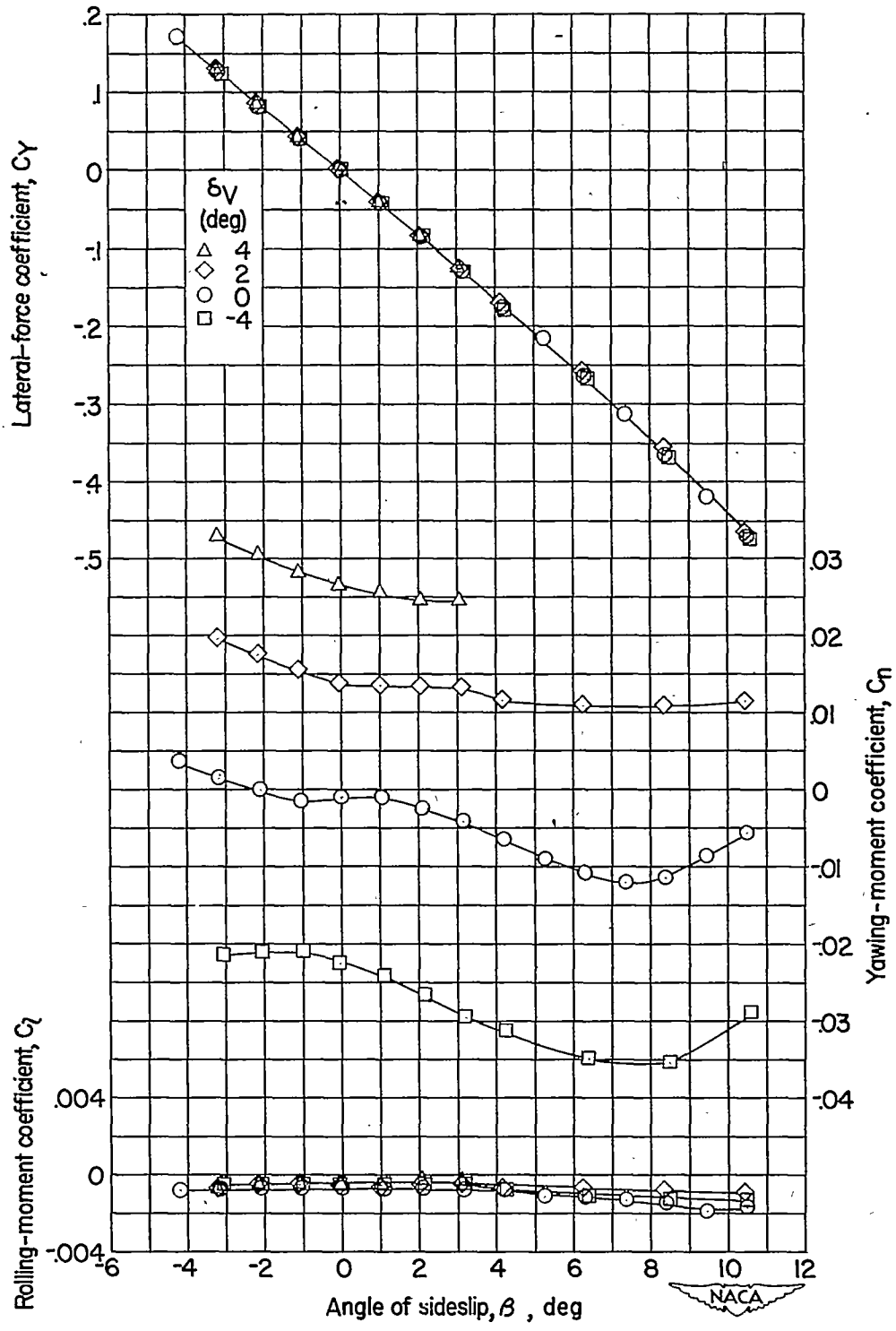

(a) C_l, C_n, and C_Y against β for several values of δ_v.

Figure 19.- Directional control characteristics of the model with large vertical canard and forward nacelle location. $\alpha = 0^{\circ}$.

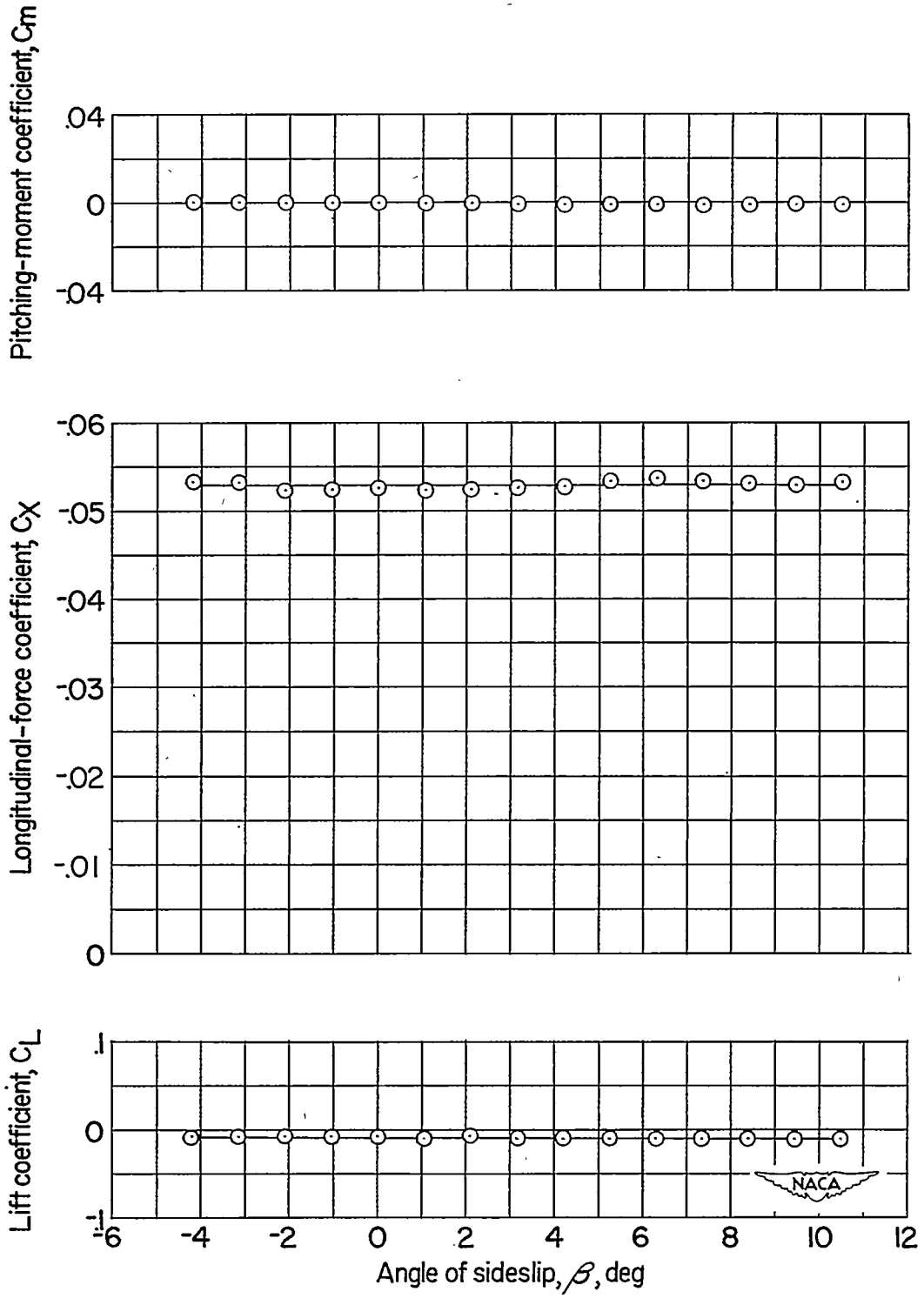

(b) C_L, C_X, C_m against β for $\delta_v = 0^\circ$.

Figure 19.- Continued.

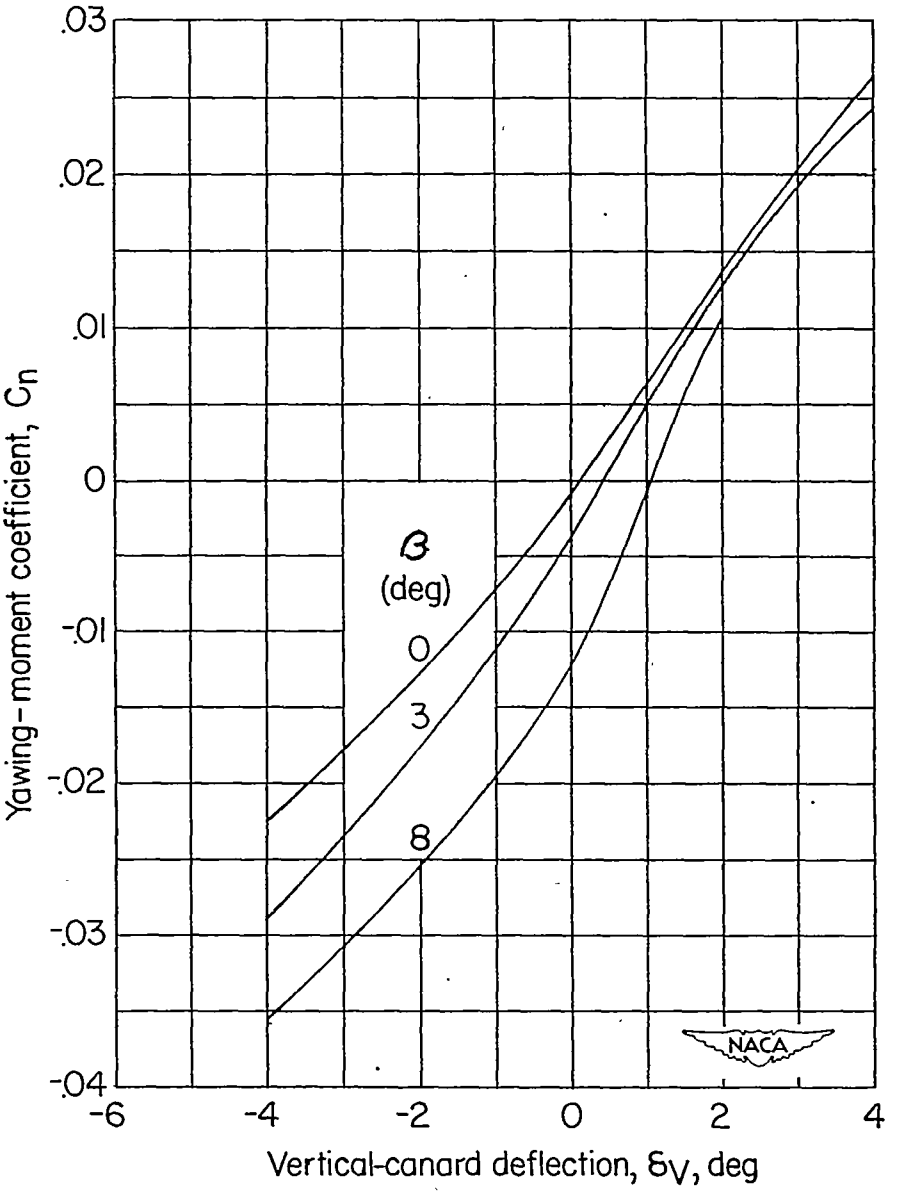

(c) C_n against δ_V for several values of β.

Figure 19.- Concluded.

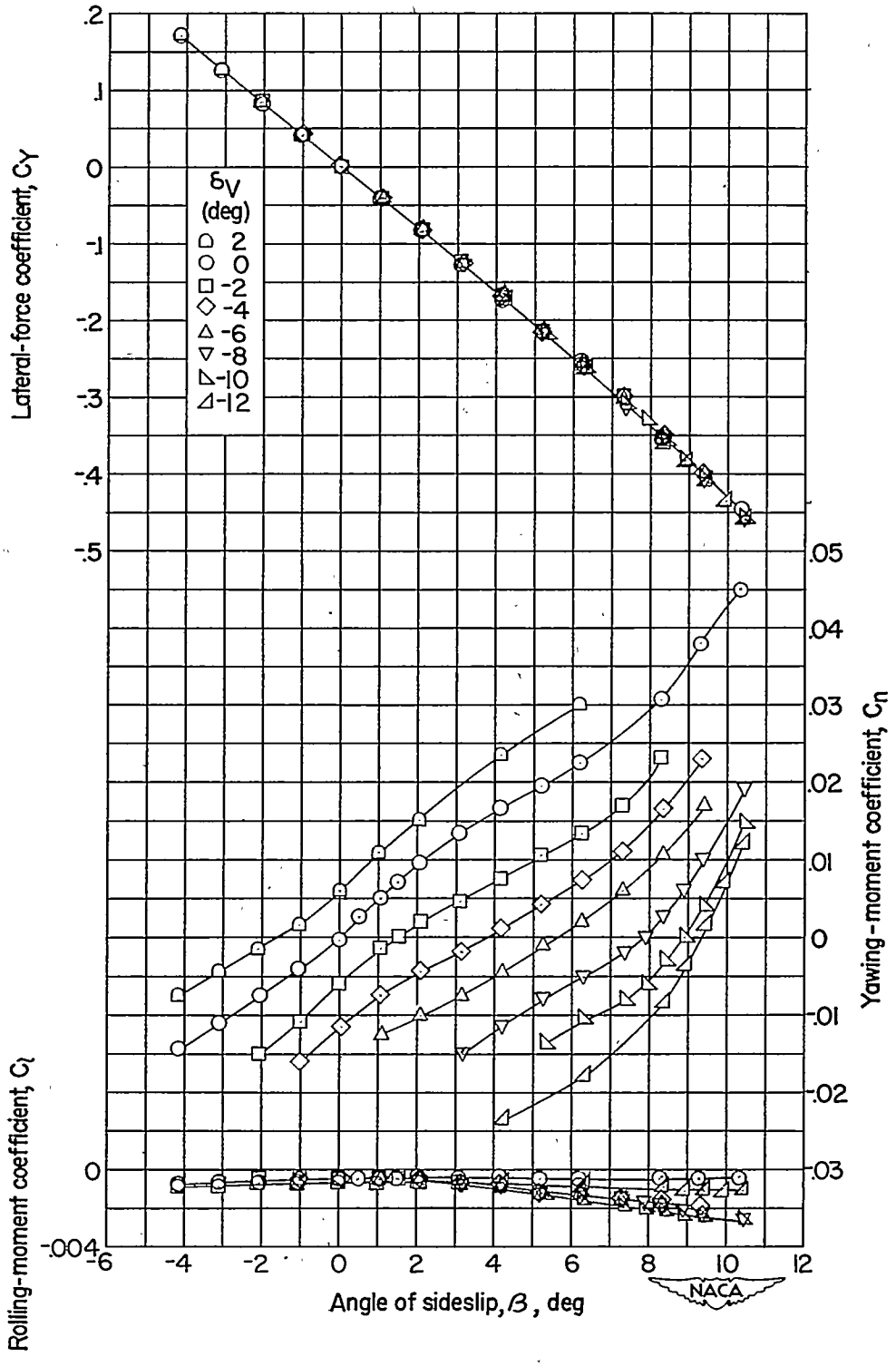

(a) $\alpha = 0^{\circ}$.

Figure 20.- Directional control characteristics of the model with small vertical canard and forward nacelle location.

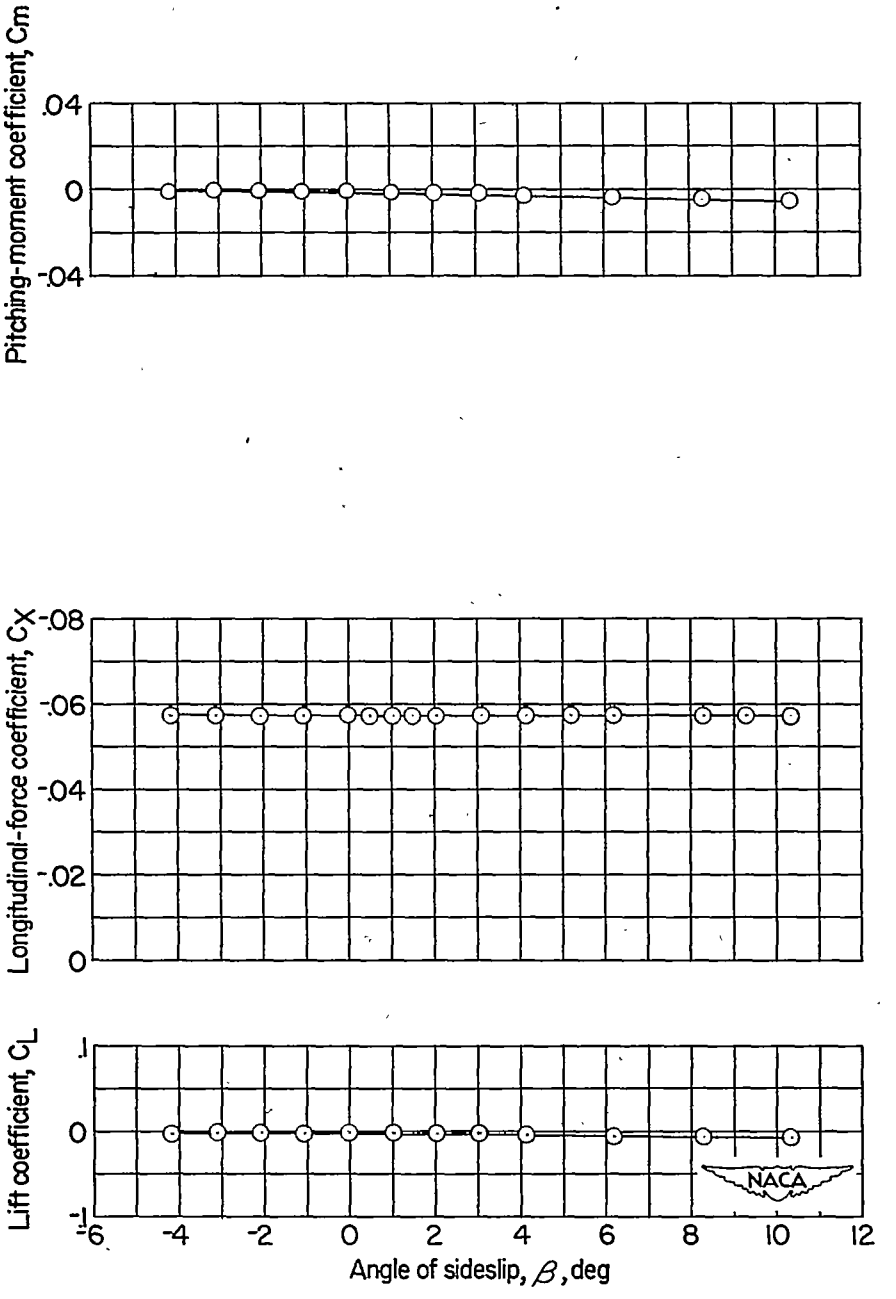

(a) Concluded.

Figure 20.- Continued.

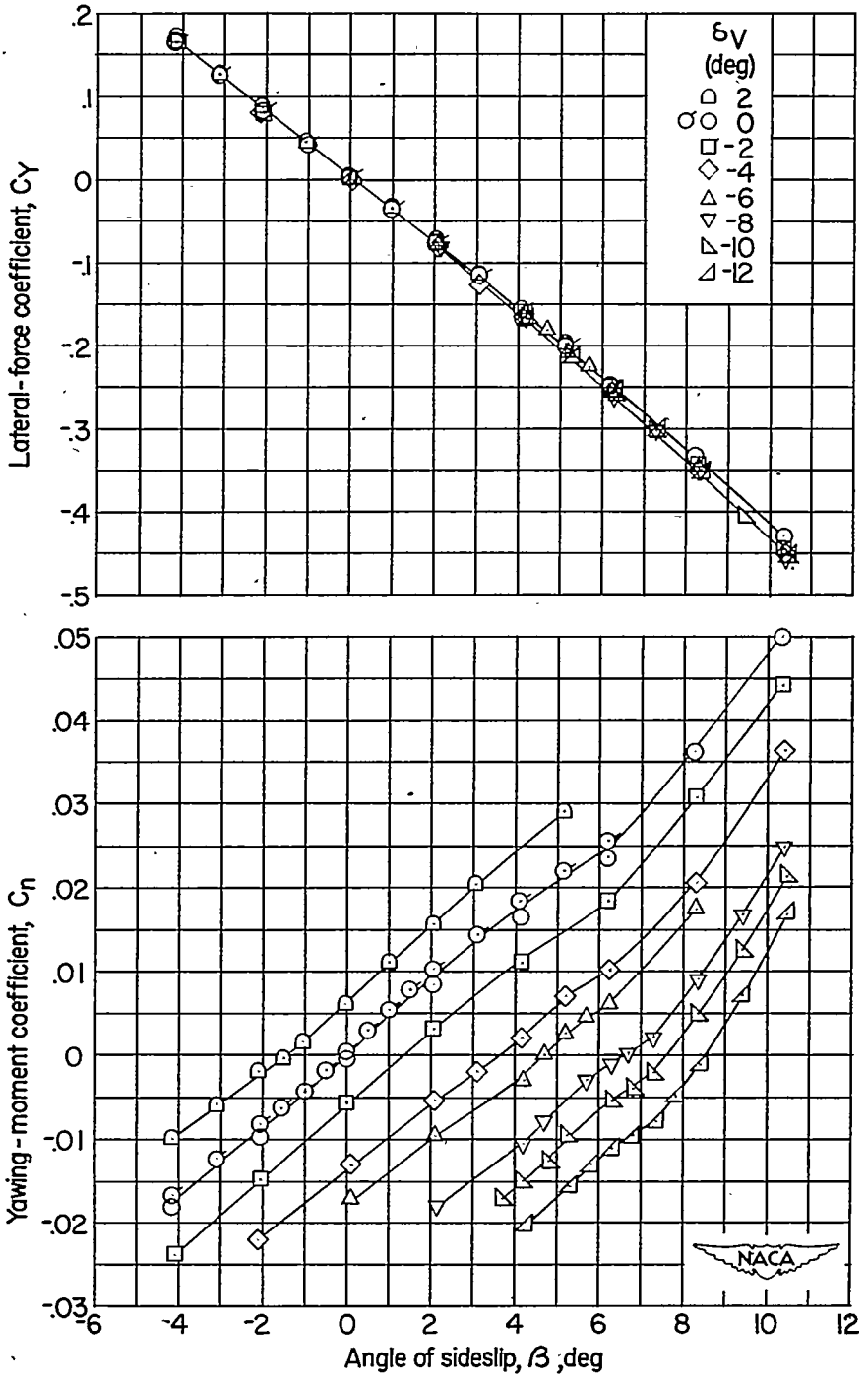

(b) $\alpha = 6.3^{\circ}$.

Figure 20.- Continued.

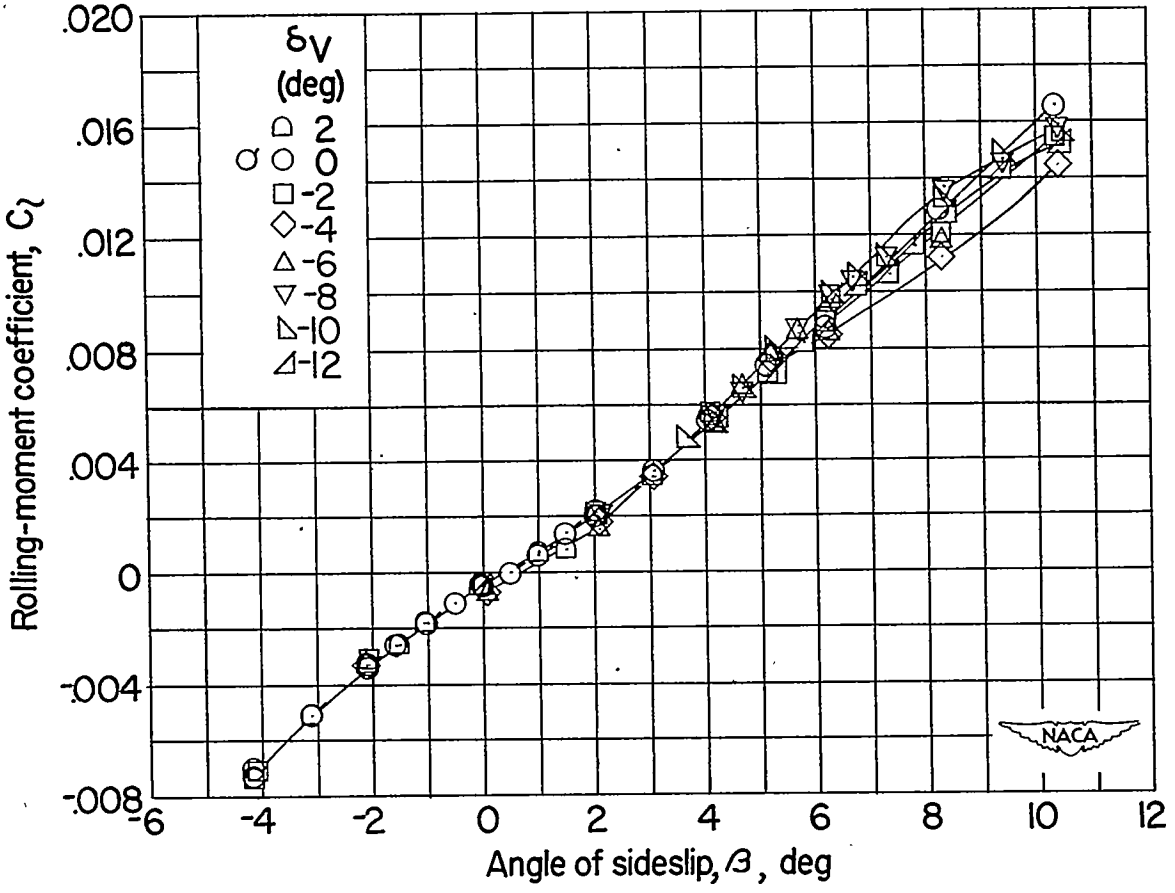

(b) Continued.

Figure 20.- Continued.

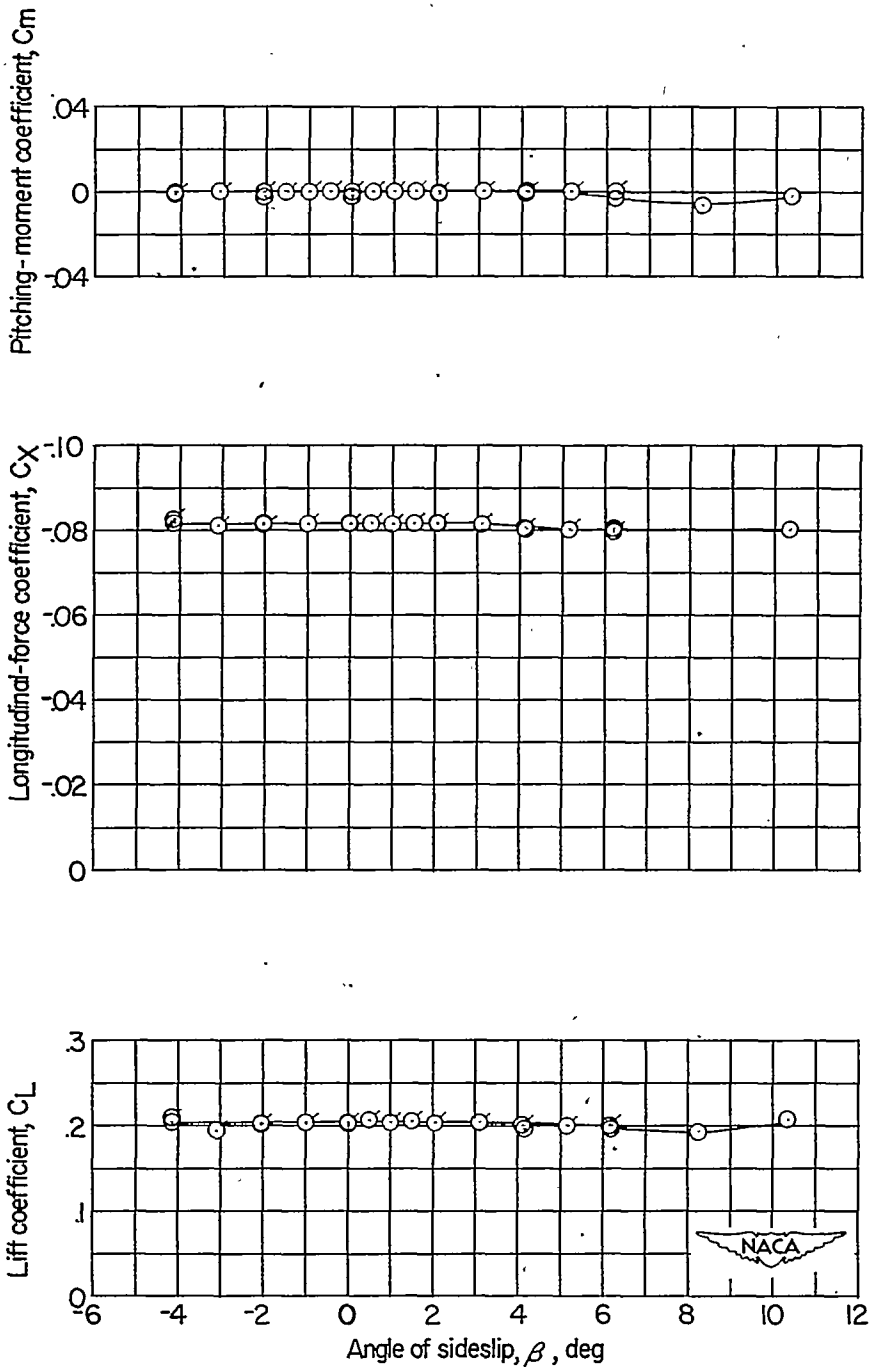

(b) Concluded.

Figure 20.- Concluded.

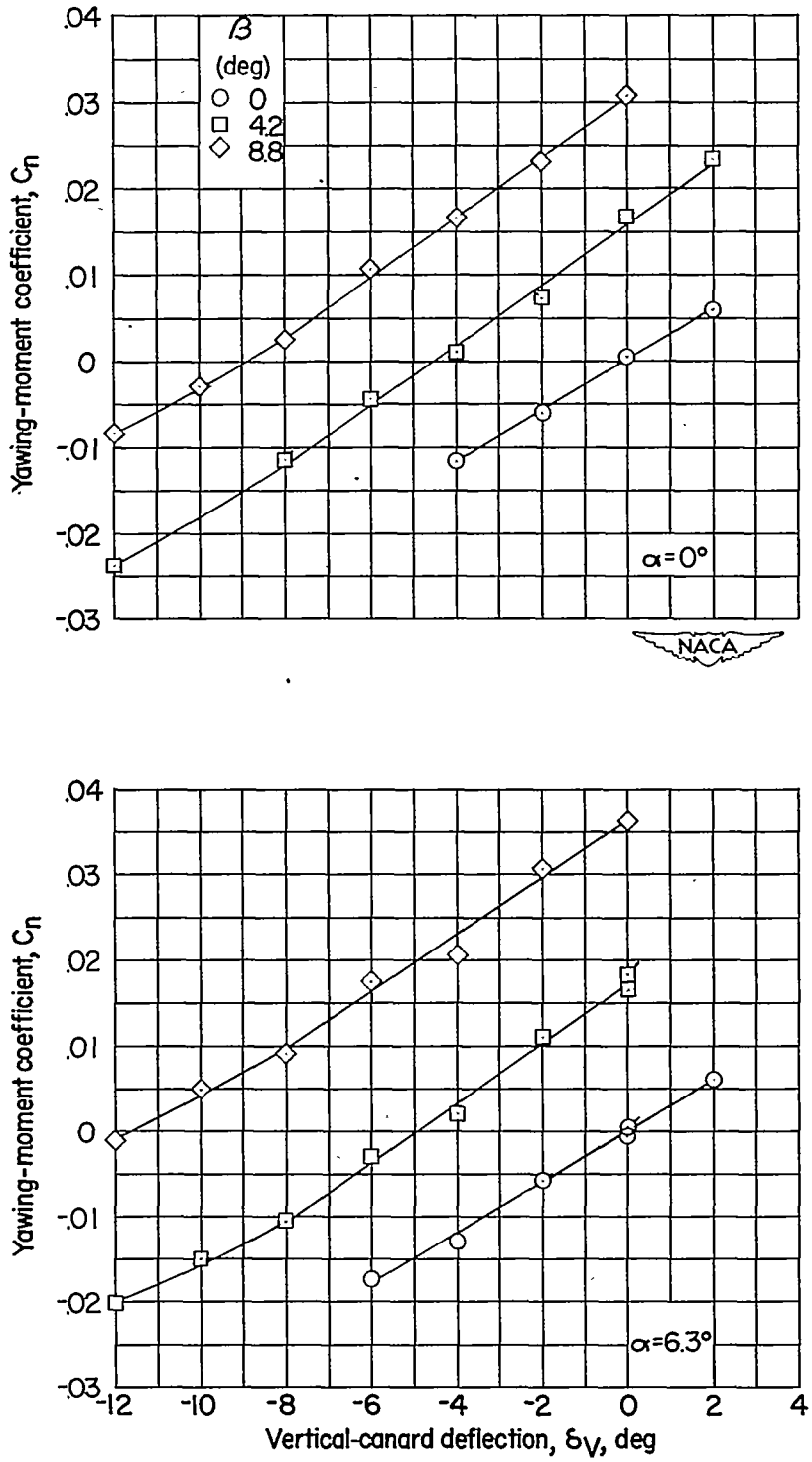

(a) C_n against δ_v for several values of β.

Figure 21.- Summary of directional control characteristics for the model with the small vertical canard and forward nacelle location.

[redacted]

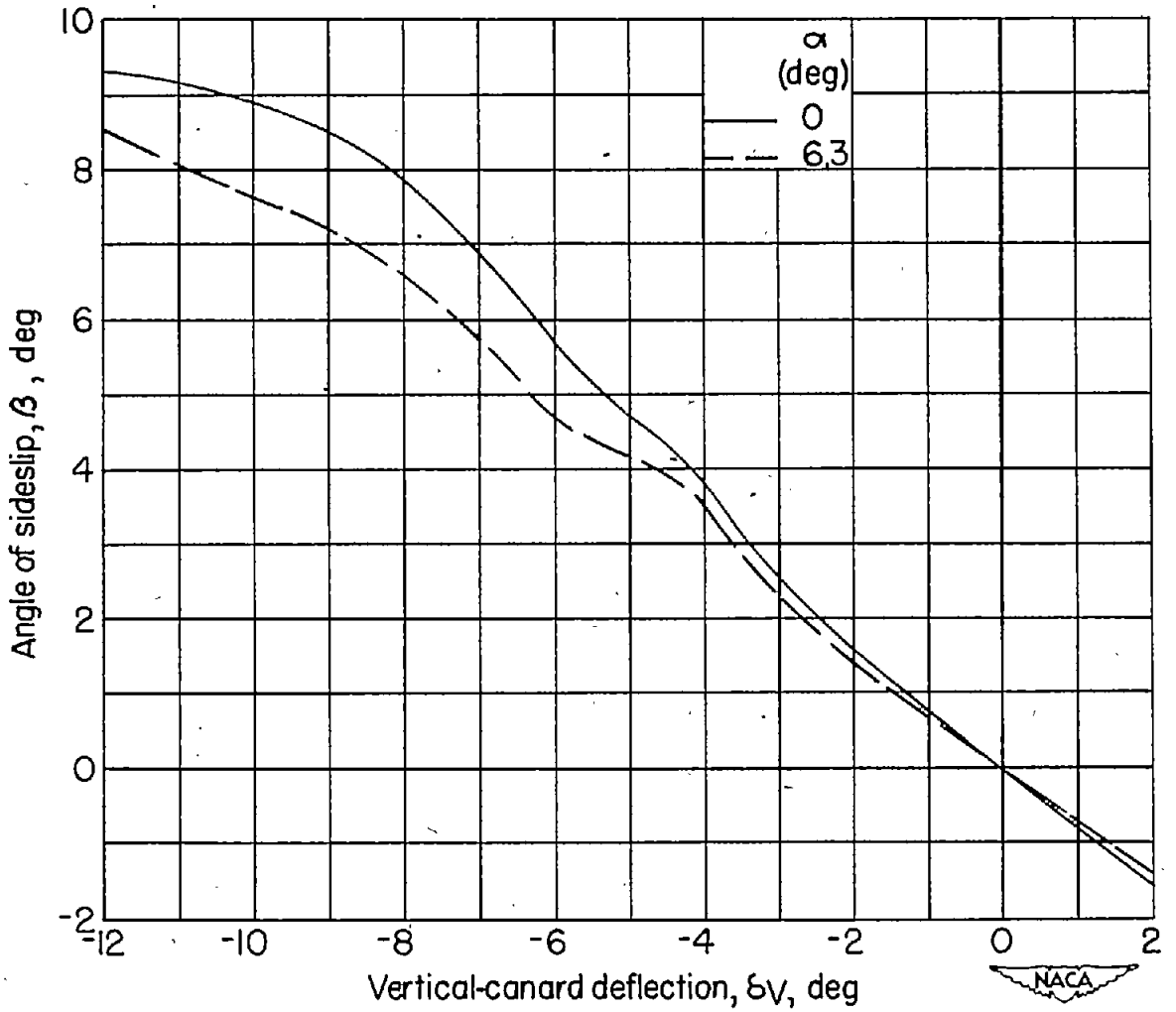

(b) β against δ_V.

Figure 21.- Concluded.

[redacted]

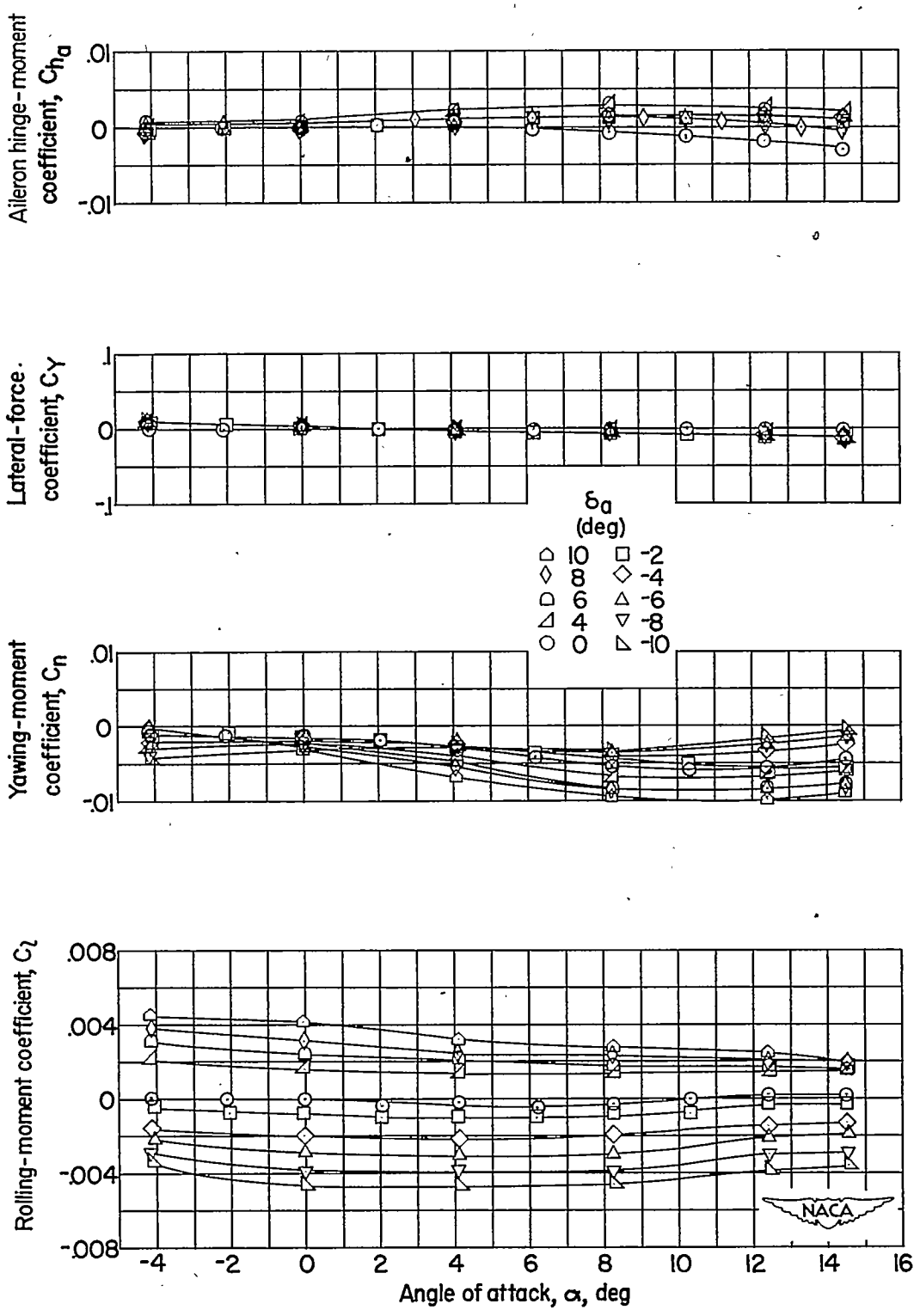

Figure 22.- Effect of aileron deflection on the aerodynamic characteristics of the model with large vertical canard and forward nacelle location.

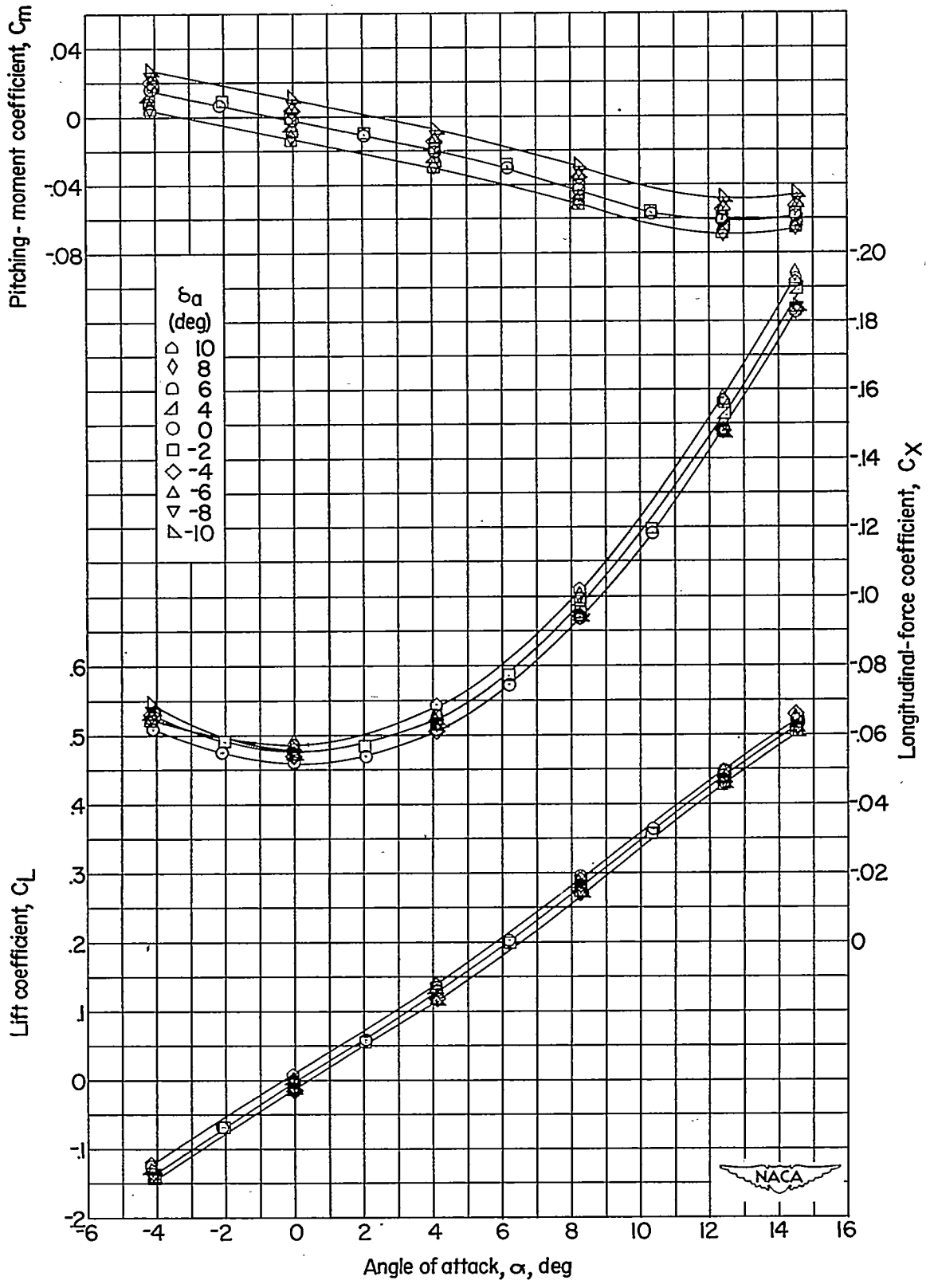

Figure 22.- Concluded.

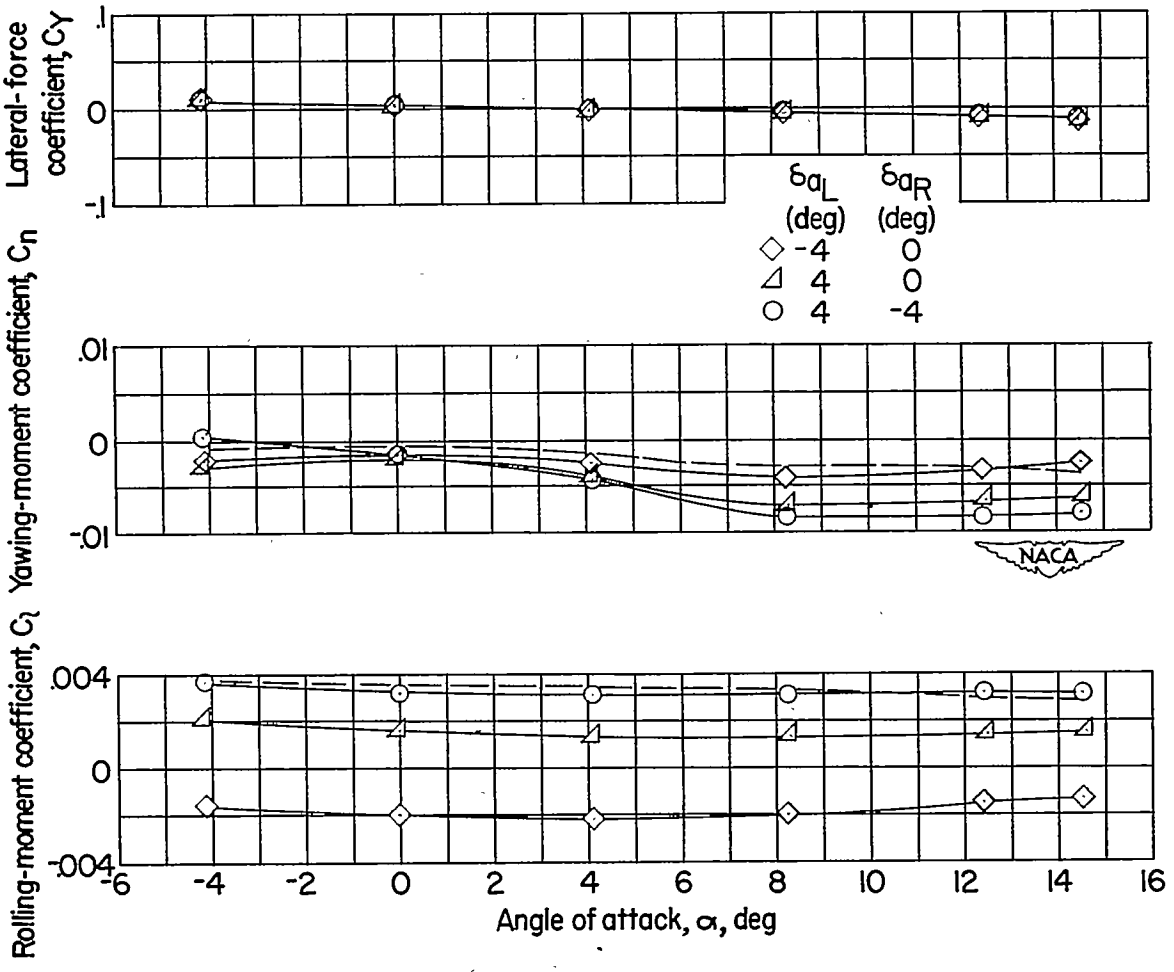

Figure 23.- Effects of simultaneous deflection of both ailerons.

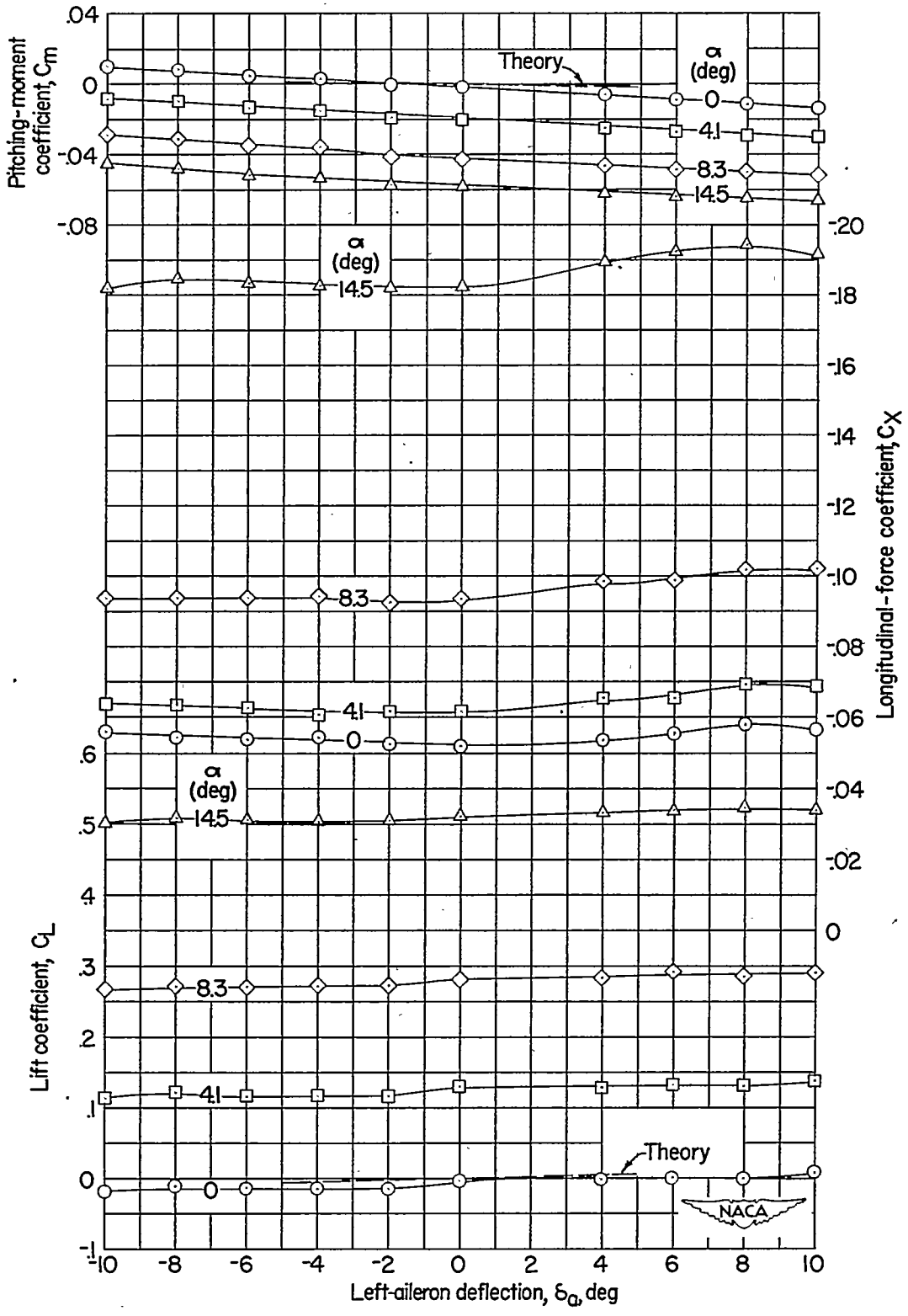

Figure 24.- Variation of aerodynamic characteristics with aileron tion for several angles of attack. Large vertical canard and nacelle location.

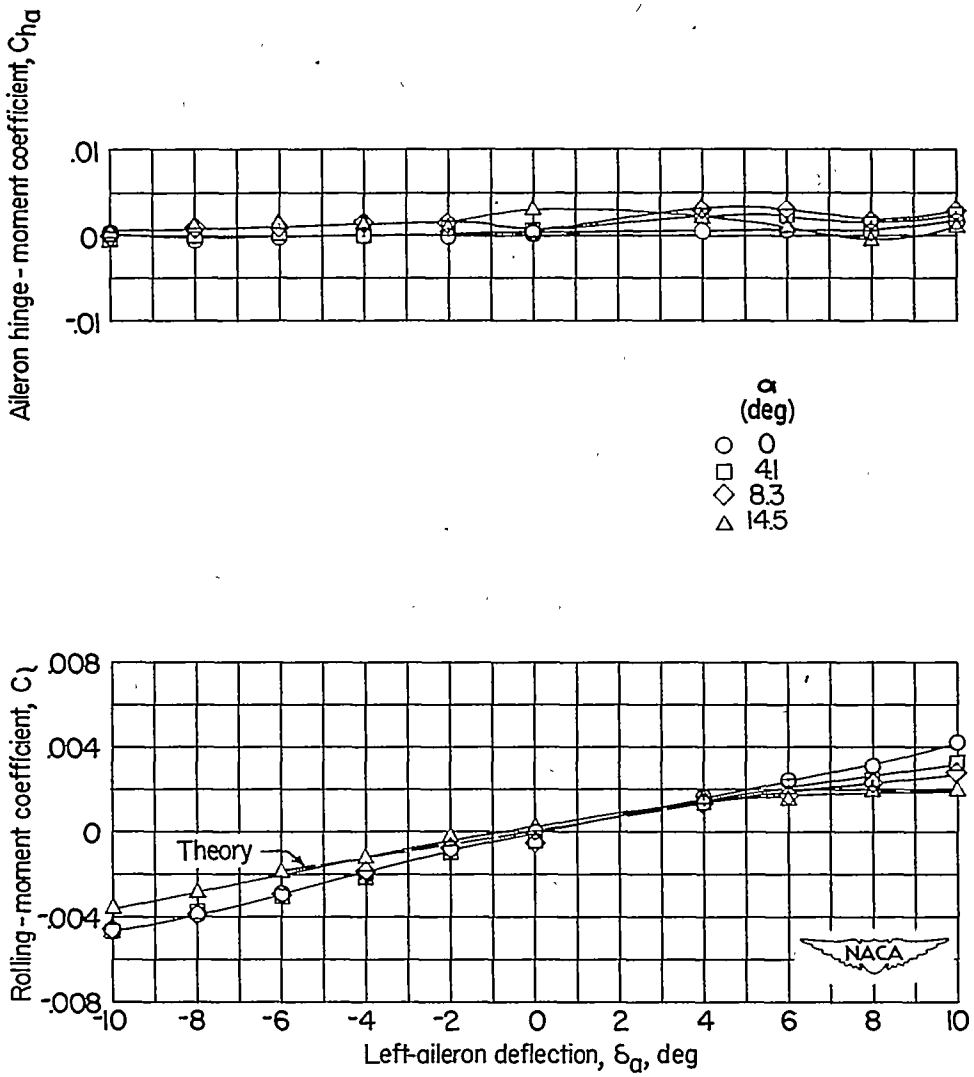

Figure 24.- Concluded.

NACA-Langley - 8-1-52 - 350